

Universität Heidelberg
Interdisciplinary Center for Scientific Computing
Engineering Mathematics and Computing Lab

Bachelor Thesis

Continuous Modeling of Extracellular Matrix Invasion by Tumor Growth

Name: Maximilian Bing

Matriculation number: 3606060

Advisor: Professor Vincent Heuveline

Date of submission: April 26, 2024

Hiermit versichere ich, dass ich die Arbeit selbst verfasst und keine anderen als die angegebenen Quellen und Hilfsmittel benutzt und wörtlich oder inhaltlich aus fremden Werken Übernommenes als fremd kenntlich gemacht habe. Ferner versichere ich, dass die übermittelte elektronische Version in Inhalt und Wortlaut mit der gedruckten Version meiner Arbeit vollständig übereinstimmt. Ich bin einverstanden, dass diese elektronische Fassung universitätsintern anhand einer Plagiatssoftware auf Plagiate überprüft wird.

Abgabedatum:

Zusammenfassung

Krebszellen können sich vom Primärtumor lösen und das umgebende Gewebe abbauen. Kontinuierliche mathematische Modelle werden verwendet, um diesen Prozess besser zu verstehen.

In diesem Zusammenhang basieren die Modelle in der Regel auf mindestens drei Schlüsselkomponenten: den Tumorzellen, dem umgebenden Gewebe oder der extrazellulären Matrix (ECM) und den matrixabbauenden Enzymen (MDE). Diese Variablen werden in dem hier behandelten Modell in einem System partieller Differentialgleichungen gekoppelt um den komplexe Prozess der Tumor Invasion zu beschreiben.

Wegen der hohen Freiheitsgraden eines solchen Modells, hat eine Konfiguration der Parameter des Modells hohen Einfluss auf die produzierten Ergebnisse. Diese Arbeit untersucht den Einfluss der Wahl dieser Konfigurationen, sowie den der Dimension, auf die Ergebnisse einer Simulation.

In der Literatur werden fast ausschließlich eindimensionalen Experimente beschrieben, daher werden die Experimente hier nur in höheren Dimensionen durchgeführt, zwei oder drei dimensional. Darüber hinaus wurde hauptsächlich die homogene Struktur der extrazellulären Matrix (ECM) behandelt, jedoch fuer eine heterogene extrazelluläre Matrix Struktur nur solche Faelle analysiert, die wenig biologische Relevanz haben. Die Struktur der epithelialen Schicht und der benachbarten extrazellulären Matrix ist jedoch in biologischem Gewebe deutlich organisierter als in den meisten später gezeigten Simulationen und anderen Beispielen aus der Literatur. Diese Organisiertheit kann zu erheblichen Veränderungen der Ergebnisse führen, selbst wenn die Parameter konstant gehalten werden.

Um realitätsnahe biologische Szenarien zu simulieren, verlangen Simulationen mindestens zwei räumlichen Dimensionen. Daher soll diese Arbeit einen Einstiegspunkt geben um das zu grundlegende Modell fuer solche Simulationen zu nutzen. Die Parameteranalyse soll hierbei auch helfen eine angebrachte Wahl der Parameter zu erleichtern.

Abstract

Cancer cells can detach from the primary tumor and degrade the surrounding tissue. Continuous mathematical models are been utilized to understand this process better.

In this context the models typically rely on at least three key components: tumor cells, the surrounding tissue or extracellular matrix (ECM), and matrix-degrading enzymes (MDE). These variables are coupled in the investigated model of in a system of partial differential equations to describe the complex process of tumor invasion.

Due to such a model's high degree of freedom, the configuration of the model parameters significantly influences the resulting outcomes. This study investigates the impact of choosing these configurations, as well as the dimensionality, on the results of a simulation.

The literature predominantly describes one-dimensional experiments; hence, the experiments conducted here are performed in higher dimensions, two—or three-dimensional. Furthermore, while the homogeneous structure of the extracellular matrix (ECM) has been mainly addressed, cases involving a heterogeneous ECM structure have been analyzed to a lesser extent despite their limited biological relevance. However, the structure of the epithelial layer and the adjacent extracellular matrix in biological tissue is more organized than in most simulations and other examples presented in the literature. This organization can lead to significant changes in results, even when parameters are held constant.

To simulate realistic biological scenarios, simulations require at least two spatial dimensions. Therefore, this work provides a starting point for utilizing the underlying model for such simulations. The parameter analysis aims to facilitate an appropriate selection of parameters.

Contents

1	Introduction	5
2	Theoretical Basics	6
2.1	Basics of Tumor Biology	6
2.2	Mathematical Methods in Oncology	8
3	Modelling	10
3.1	Mathematical Formulation	10
3.2	Numerical Formulation and Parameters	11
4	Experiments and Results	13
4.1	2D Results without Proliferation and Renewal - Homogenous ECM	14
4.1.1	Basecase Analysis	16
4.1.2	Parameter Analysis	19
4.2	2D Results with Proliferation and Renewal - Homogenous ECM	39
4.2.1	Basecase Analysis	41
4.2.2	Parameter Analysis	41
4.3	3D Results with Proliferation and Renewal - Homogenous ECM	54
4.3.1	Basecase Analysis	54
4.3.2	Parameter Analysis	54
4.4	2D Results with Proliferation and Renewal - Heterogenous ECM	54
4.5	3D Results with Proliferation and Renewal - Heterogenous ECM	57
5	Conclusion and Discussion	58

1 Introduction

Modeling tumor growth plays a crucial role in understanding the complex mechanisms governing the development and progression of cancer diseases. Since cancer is one of the leading death causes worldwide, and many of its forms are incurable, challenges in the area of Oncology require researchers to have a deep understanding in the biological foundation, which leads to malignant cell mutation and factors for tumor growth and spreading, as well as the mathematical models used for simulating these events. This Bachelor thesis is dedicated to analyzing Anderson et al.'s [1, 2] model for tumor modeling.

The dynamics of tumorous growth are an intricate system influenced by numerous biological and chemical factors, genetic pre-dispositions, the surrounding tissue of cancer cells, angiogenic processes, and interactions with the immune system. Integrating these factors in mathematical models allows us to decode these complex interactions with quantification and helps us understand the fundamental mechanisms surrounding cancerous diseases.

Mathematical models are an essential part of Oncology; they are used to quantify biological phenomena and help predict and understand tumor development and treatment response. In Mathematical Oncology, we differentiate between continuous, discrete, and hybrid models [3]; for the continuous type, cells and tissue are described over time with partial differential equations modeling continuous quantities like, in our case, tumor cell density or extracellular matrix concentration.

In the discrete case, an entity-based model is used, pursued with the goal of better understanding the phenomena on the cell level. This approach allows the researcher to better implement a cell's biological effects with its outer circumstances, like interaction with other cells, nutrients, or other microorganisms. As the name implies, use these models' discrete values to describe the temporal course of events.

Hybrid models try to combine both approaches, to offer efficient systems capturing cell level events and continuous changes in outer circumstances.

This work investigates how a continuous model proposed by Anderson et al. [1, 2] to analyze tumor development in the early stages of a cancer disease performs in the case of different dimensions and free parameter values. The model examines the first two stages of a cancer disease: tumor initiation, where the tumor cells are localized to a small area and have not yet spread throughout the body, and tumor promotion, with the tumor cells growing and proliferating, invading the surrounding tissue [4]. From examples of the original paper, we can already see that the model's results vary with the dimensionality of the space, we are modeling the partial differential equations in. Our primary focus is comparing simulations of two dimensions with those of three dimensions of extracellular matrix invasion by tumor growth.

Additionally to the variation of dimensions, we will briefly examine how the geometry of the extracellular matrix will influence tumor development.

Another point of interest is investigating how the model's free parameters influence tumor dynamics growth. An important task is to give those parameters a biological meaning and eventually gain insight into how to adjust them to make the simulation more realistic.

2 Theoretical Basics

2.1 Basics of Tumor Biology

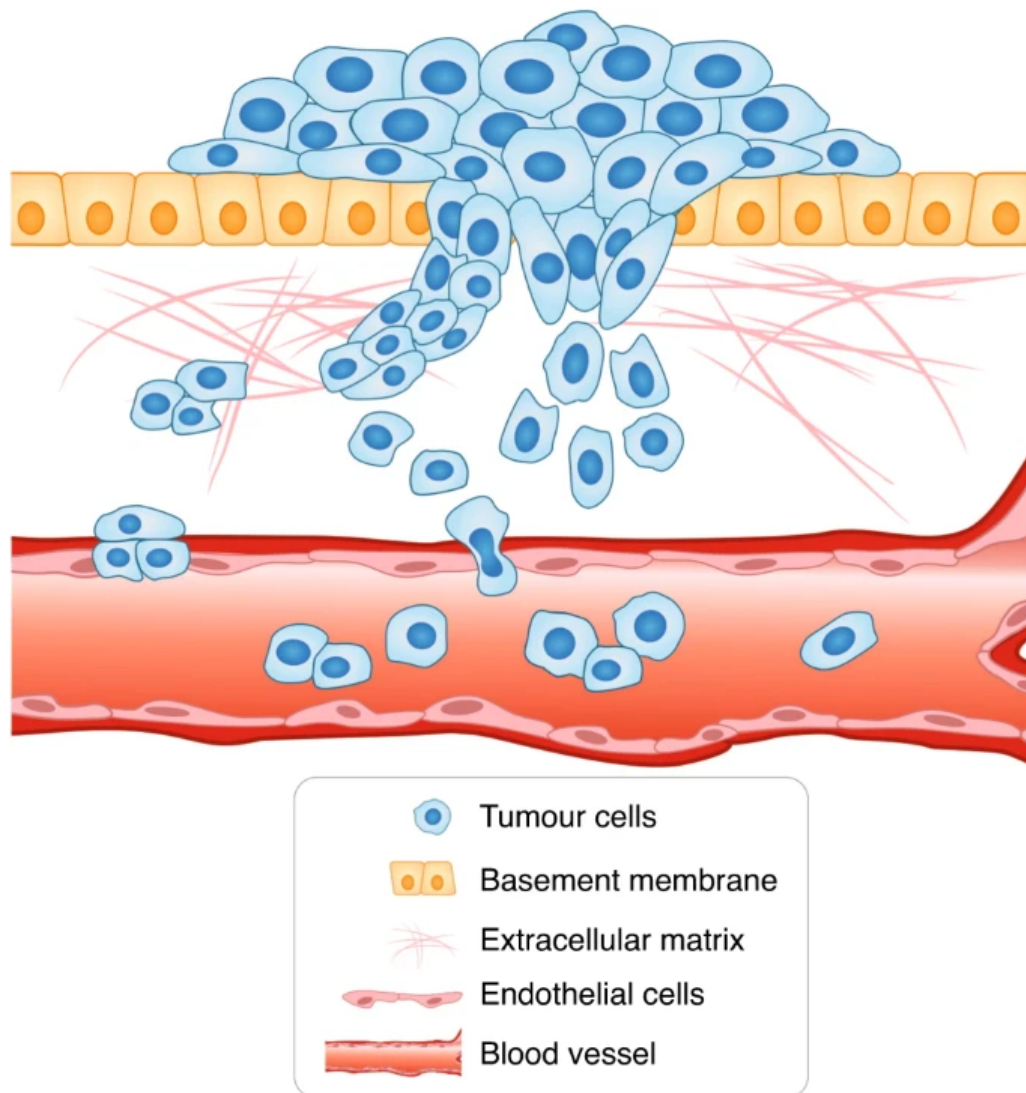


FIGURE 1. Tumor Invasion Stage

The body of a living creature is made up of more than 200 different types of cells; the coordination between the cells and their surroundings keeps the body running. Each of these cells is built from the genetic information encoded in the DNA in the cells' nuclei. Though the nucleotide sequence of DNA is well-checked and maintained throughout the cell's life, mutations still occur that cause changes in a cell's DNA. These mutations may be of a positive, negative, or neutral nature. In the case of a harmful mutation, this alternation of the DNA may cause diseases, with cancer being one of them. The failure of the complex system managing cell birth, proliferation, and cell death (apoptosis) causes cancer, resulting in uncontrolled cell proliferation in a local area. A conglomeration of

cancer cells is called a tumor.

Cancer diseases can be categorized medically into five stages. First is the tumor initiation phase, where it comes to the above explained genetic mutations of normal cells. The next stage is the tumor promotion stage, in which the mutated cells of phase one may experience further genetic alterations resulting from uncontrolled growth and proliferation of the cancerous cells. The third stage is the tumor progression stage, where the cancerous cells progress in growing and proliferating, reaching a critical mass, and forming a tumor at a local site of the body. Fourth comes the invasion stage, shown in figure 1. Here, the tumor can invade surrounding tissue by breaking through the cellular membrane, invading the extracellular matrix inside, and entering the blood circulation or lymphatic systems. Next, the tumor cells that have invaded the blood circulation of the lymphatic system spread throughout the body and form new tumors. This stage is called Metastization. To grow tumors further, they need access to nutrients and oxygen. During angiogenesis, a tumor develops its own blood vessels, securing its nutritional provision. At this stage, the first symptoms of the host may appear, enabling medical treatment.

In our model, the focus lies on the first two stages: tumor invasion and tumor progression. The tumor invasion stage is characterized by the malignant cells gaining the ability to penetrate and invade the surrounding tissue. The tumor cells break through the normal tissue barrier and infiltrate neighboring structures. In order to do so, the cancer cells produce so-called matrix-degrading enzymes which break down the extracellular matrix. The degradation of the extracellular matrix helps local spreading and destroys otherwise healthy tissue and cells in the affected area. In the next phase, the tumor progression stage, the tumor has grown more extensive, and the cancerous cells take on more aggressive behavior by invading the surrounding area further. While they keep growing uncontrolled, they are also affected by further genetic instabilities, which lead to more mutations, possibly developing resistance mechanisms against, for example, degrading factors. Already in this stage, the affected area is exposed to heavy tissue damage and functional disabilities.

The most important factors influencing those two phases are the genetic dispositions of the tumor cells towards proliferation and the evasion of apoptosis, programmed cell death, which increase the invasive potential. Another critical factor is the geometry of the extracellular matrix, as well as the exact macromolecules that make it up. A solid immune biological defense reaction also helps the body defend against spreading cancer cells. Hence, evasion of detection and destruction of the tumor cells plays a vital role in the first stages. To invade the affected area, the malignant cells need to be able to move freely and quickly. In order to do so, cancer cells can gain the ability to lose adhesion properties, which healthy cells usually have, to allow migrating into the surrounding tissue. Another organization principle for cancerous diseases is found in the Hallmarks of cancer, 2, of Douglas Hanahan and Robert Weinberg [4]. They describe a set of functional capabilities, eight hallmark capabilities, and two enabling characteristics commonly acquired by cancer cells. They contribute to their ability to grow uncontrollably, evade the immune system, and metastasize. These hallmarks are sustaining proliferative signaling, evading growth suppressors, avoiding immune destruction, enabling replicative immortality, tumor-promoting inflammation, activating invasion and Metastization, inducing or

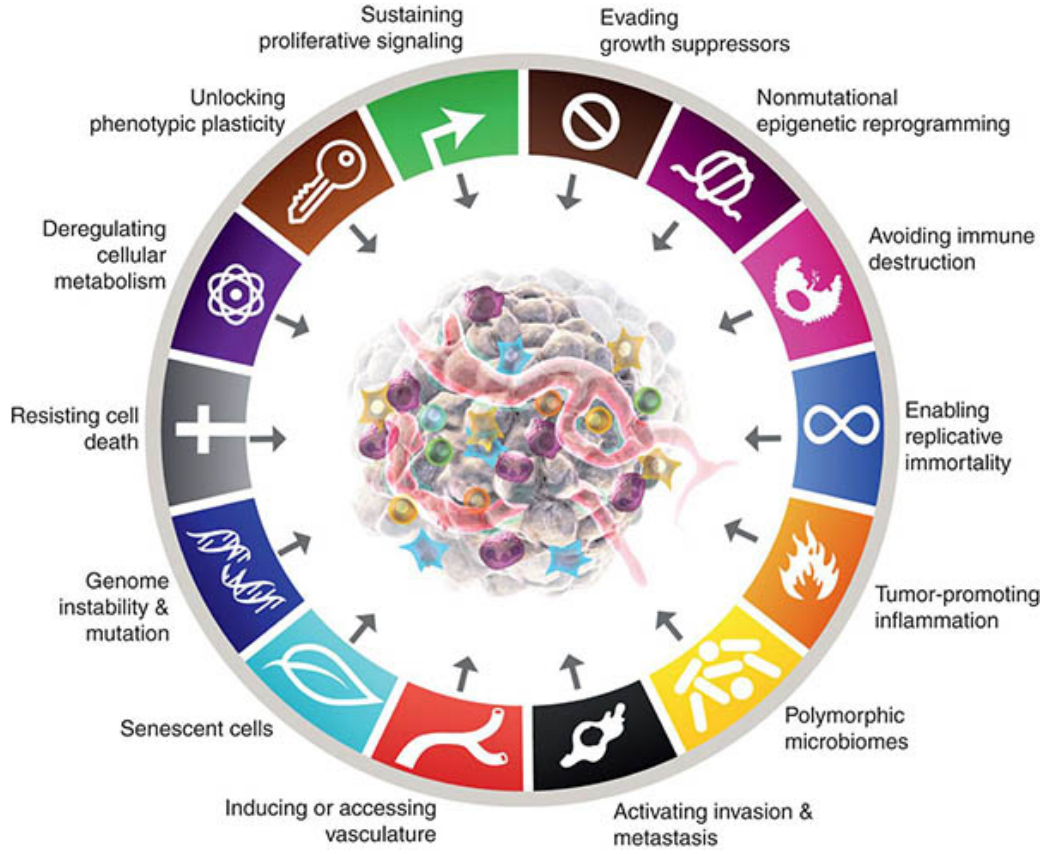


FIGURE 2. Hallmarks of Cancer

accessing vasculature, genome instability and mutation, resisting cell death, deregulating cellular metabolism. These Hallmarks of Cancer together contribute to the development and progression of cancer and provide targets for therapeutic intervention and research efforts aimed at understanding and treating the disease.

In our model, we see many of the capabilities incorporated. Proliferative signaling only relies on the tumor cells themselves and not on typically other hormones or molecules, allowing them to proliferate rapidly without external growth signals. Immune destruction and induced cell death are avoided, optimizing them to survive and accumulate genetic mutations that promote tumor growth. The tumor cells can invade the surrounding tissue, modeled by the extracellular matrix.

2.2 Mathematical Methods in Oncology

Mathematical methods and models in Oncology play a crucial role in analyzing, understanding, and predicting cancer development. Since the objective of this research underlies complex and intricate biochemical systems and mechanisms, many models exist that find their respective applications in distinct areas of this research field. These methods can be coarsely divided into three sections: continuous, discrete, and hybrid models [3]; for describing tumor growth, exponential and logistic growth models are often used, the latter

allowing limiting factors to play a role during modeling. These methods are a subclass of the differential equations approach, which bases their functionality on an ordinary or partial differential equation, studying the continuous approach. Like our model, they are not limited to only one equation but can include many, incorporating systematic dependencies on other factors. These models generally deal with continuous quantities like densities or concentrations, for example, spatial and temporal nutritional supply or drug concentration, as well as their effects on the affected area over time. Discrete models use discrete entities to describe the behavior of tumor cells and their interactions with surrounding tissue. They allow us to model a wide range of biological and chemical processes which are hard to describe continuously. Commonly used types in mathematical oncology are, for example, Cellular Automata or Agent-Based Models. Cellular Automata represents cells as entities with states on a grid, with each cell being allowed to change states according to a set of rules based on its own current state and the states of the neighbors.

In contrast, Agent-Based Models enable the differentiation of cell types and allow movement that is not restricted to a grid, implementing complex mechanics at cell-cell or cell-environment levels. Using these discrete models allows researchers to focus on biological effects during modeling, which are hard to describe in continuous models. With these approaches, we can simulate genetic and evolutionary events. For example, they are studying the genetic alternations of tumor cells or the interaction between healthy and cancerous cells.

Hybrid models combine both methods above, using continuous and discrete approaches. Like in the model proposed by Franssen et al. [5] or Anderson et al. [1], these approaches allow to incorporate the exactness of continuous models with a wide range of biological effects described by discrete models.

However, not all models try to model tumor growth; others are concerned with optimality regarding drug dosages or radiation exposition, offering personalized treatment, or Machine Learning and Data Mining methods analyzing large datasets to identify patterns and predict outcomes. The latter method may be used in all kinds of applications, for example, spacial or temporal cancer development, as well as drug dosage optimization for individual patients. Putting all these methods together gives us a powerful toolbox to simulate and understand cancer biology. As the last years have shown, they are applied in a wide range of areas, offering insight into all areas of cancer research. Therefore, it is essential to come up with methods and evaluate their usefulness and meaningfulness in different research areas.

3 Modelling

3.1 Mathematical Formulation

The model proposed by Anderson et al. [1, 2] and Chaplain et al. [1, 5, 6], extended with terms for modeling cell proliferation and extracellular matrix renewal consists of a system of coupled partial differential equations with zero-flux boundary conditions:

$$\frac{\partial c}{\partial t} = D_c \Delta c - \chi \nabla \cdot (c \nabla e) + \mu_1 c \left(1 - \frac{c}{c_0} - \frac{e}{e_0} \right) \quad (1)$$

$$\frac{\partial e}{\partial t} = -\delta m e + \mu_2 c \left(1 - \frac{c}{c_0} - \frac{e}{e_0} \right) \quad (2)$$

$$\frac{\partial m}{\partial t} = D_m \Delta c + \mu_3 c - \lambda m \quad (3)$$

$$\zeta \cdot (-D_c \nabla c + c \chi \nabla e) = 0 \quad (4)$$

$$\zeta \cdot (-D_m \nabla m) = 0 \quad (5)$$

with the free parameters D_c , D_m , χ , δ , μ_1 , μ_2 , μ_3 and λ .

The variable c describes the tumor cell density, e the concentration of the extracellular matrix, and m the matrix-degrading enzyme concentration. All of those functions are mathematically defined to be mapping a 1,2 or 3-dimensional spacial value x and a temporal value t to a scalar value describing the respective quantity at a specific point in space and time (x, t) , $\{c, e, m\} : \mathbb{R}^3 \times \mathbb{R} \rightarrow \mathbb{R}$.

To derive the expression of the tumor cell density c , we are going to assume that the tumor cell's movement is subject to two influences: haptotaxis and random movement. Haptotaxis is a directed migratory response of cells to gradients of fixed or bound chemicals [1], and random movement is influenced by, for example, mechanical stress, electric charge or other such physical effects [7]. We must define flux to get an expression of how much or how fast the tumor cells move. Flux is defined to be the amount of a substance that crosses a unit area in a unit time. Incorporating the two assumed influencing factors into our mathematical model; we define the haptotactic flux J_{hapto} and random flux J_{random} :

$$J_{hapto} = \chi c \nabla e$$

$$J_{random} = -D_c \nabla c$$

χ is the haptotactic flux coefficient and D_c is a random mobility coefficient. These parameters could also be a function of, for example, extracellular matrix and or matrix-degrading enzyme concentration. Knowing that cells grow over time and proliferate, we want to respect this in our model with a term for tumor cell proliferation: $\mu_1 c (1 - \frac{c}{c_0} - \frac{e}{e_0})$.

The idea is that this term describes the cell proliferation with a logistic growth model respecting spacial limiting factors of already present extracellular matrix molecules and tumor cells, μ_1 describes the rate at which proliferation happens. In the initial model proposed by Anderson et al. [1, 2] and Chaplain et al. [1, 5, 6, 8], they did not respect

proliferation of tumor cells and extracellular matrix renewal. They applied a conservation equation for the tumor cells, which yields:

$$\begin{aligned}\frac{\partial c}{\partial t} &= -\nabla \cdot (J_{hapto} + J_{random}) \\ \frac{\partial c}{\partial t} &= -\nabla \cdot (\chi c \nabla e - D_c \nabla c) \\ \frac{\partial c}{\partial t} &= D_c \Delta c - \chi \nabla \cdot (c \nabla e)\end{aligned}$$

The extended model incorporates proliferation and renewal into this conservation formula, resulting in equation 1:

$$\begin{aligned}\frac{\partial c}{\partial t} &= -\nabla \cdot (J_{hapto} + J_{random}) + \mu_1 c \left(1 - \frac{c}{c_0} - \frac{e}{e_0}\right) \\ \frac{\partial c}{\partial t} &= D_c \Delta c - \chi \nabla \cdot (c \nabla e) + \mu_1 c \left(1 - \frac{c}{c_0} - \frac{e}{e_0}\right)\end{aligned}$$

To model the extracellular-matrix concentration e , we assume that the enzymes degrade the extracellular matrix upon contact. The equation models this assumption:

$$\frac{\partial e}{\partial t} = -\delta m e$$

where δ is a positive constant describing this degradation process. For the extended model we add a term describing the renewal process of the extracellular matrix:

$$\frac{\partial e}{\partial t} = -\delta m e + \mu_2 c \left(1 - \frac{c}{c_0} - \frac{e}{e_0}\right)$$

with μ_2 being the coefficient describing the rate of the renewal process.

Modeling the matrix-degrading enzyme concentration m , we combine a diffusion term with production and decay terms. The diffusion term is described like in tumor cell concentration, with the addition that haptotactic fluxes are neglected and only random mobility is assumed, $J_{random} = -D_m \nabla m$. The production term depends on the tumor cell density c and the decay term on the extracellular matrix concentration m . Incorporating this gives us equation 3:

$$\begin{aligned}\frac{\partial m}{\partial t} &= \nabla \cdot J_{random} + \mu_3 c - \lambda m \\ \frac{\partial m}{\partial t} &= D_m \Delta m + \mu_3 c - \lambda m\end{aligned}$$

μ_3 and λ describing production and decay coefficients.

3.2 Numerical Formulation and Parameters

To make solving the model easier, we will first non-dimensionalize all the equations 1 to 5 in a standard way to rescale the space domain to a unit size domain Ω . For one space

dimension this results in the unit interval $[0, 1]$, for two the unit square $[0, 1] \times [0, 1]$ and for three spacial dimensions the unit cube $[0, 1] \times [0, 1] \times [0, 1]$.

We start with non-dimensionalizing the three continuous variables c, e, m :

$$\begin{aligned}\tilde{c} &= \frac{c}{c_0} \\ \tilde{e} &= \frac{e}{e_0} \\ \tilde{m} &= \frac{m}{m_0}\end{aligned}$$

Next we rescale distance with an appropriate length scale L and time with $\tau = \frac{L^2}{D}$ [2], which will be described more detailed in section. 4

Modifying the system's free parameters $D_c, \chi, \delta, D_m, \mu_3, \lambda$ gives us:

$$d_c = \frac{D_c}{D}, \quad \gamma = \chi \frac{e_0}{D}, \quad \eta = \tau m_0 \delta, \quad d_m = \frac{D_m}{D}, \quad \alpha = \tau \mu_3 \frac{c_0}{m_0}, \quad \beta = \tau \lambda.$$

with D being the reference chemical diffusion coefficient.

These modifications make the new system of coupled partial differential equations, where the tildes are dropped, and we assume t as τ for simplicities' sake, with also updated zero-flux boundary conditions:

$$\frac{\partial c}{\partial t} = d_c \Delta c - \gamma \nabla \cdot (c \nabla e) + \mu_1 c \left(1 - \frac{c}{c_0} - \frac{e}{e_0} \right) \quad (6)$$

$$\frac{\partial e}{\partial t} = -\eta m e + \mu_2 e \left(1 - \frac{c}{c_0} - \frac{e}{e_0} \right) \quad (7)$$

$$\frac{\partial m}{\partial t} = d_m \Delta c + \alpha c - \beta m \quad (8)$$

$$\zeta \cdot (-d_c \nabla c + c \gamma \nabla e) = 0 \quad (9)$$

$$\zeta \cdot (-d_m \nabla m) = 0 \quad (10)$$

where ζ is an outward unit normal vector.

In order to use the Finite Element Method, we will change to the variational formulation. If we assume each species to be in the Hilbert space $H^1(\Omega)$, the variational formulation can be derived by multiplying with a test function φ_i , integrating over the domain Ω and using integration by parts and the Gauss theorem. Using the variational formulation will give us a broader solution space and reduce the solution's requirements regarding differentiability. With (\cdot, \cdot) denoting the L^2 -scalar product on Ω the following equation system results:

$$\left(\frac{\partial c}{\partial t}, \varphi_c \right) = -d_c (\nabla c, \nabla \varphi_c) + \gamma (c \nabla e, \nabla \varphi_c) + \mu_1 \left(c \left(1 - \frac{c}{c_0} - \frac{e}{e_0} \right), \varphi_c \right) \quad (11)$$

$$\left(\frac{\partial e}{\partial t}, \varphi_e \right) = -\eta (m e, \varphi_e) + \mu_2 \left(e \left(1 - \frac{c}{c_0} - \frac{e}{e_0} \right), \varphi_e \right) \quad (12)$$

$$\left(\frac{\partial m}{\partial t}, \varphi_m \right) = -d_m (\nabla m, \nabla \varphi_m) + \alpha (c, \varphi_m) - \beta (m, \varphi_m) \quad (13)$$

4 Experiments and Results

All experiments considering the ECM homogenous start with the same initial values as seen in figure 3. Experiments observing the effects of a heterogenous ECM use different initial values, as seen in figure 35.

Solving the numerical model HiFlow³[9] will be used with the weak form given with equations 11 - 13. ParaView [10] is used to evaluate the numerical simulation results, producing informative plots to compare the evolution of the simulation in time. For this, we rely on the tool Plot Over Line to give results for the three variables of tumor cell density, extracellular matrix density, and matrix-degrading enzyme concentration. This tool also allows us to compare all three variables in one plot, whereas using 2D plots, we would need one for each variable. Using it makes the results better readable and allows a clearer quantitative insight into the experiments, as shown in figure 5.

This work starts with replicating numerical simulations done by other papers in higher dimensions. Since there were only 1D simulations done previously, the model will be adjusted so that the Plot Over Line graphs mimic the plots given by the previous experiments. This will serve two purposes: first, it will verify the correct implementation of the model, and second, it will give us a starting point by which we can vary the parameters, investigating the phenomena this model exhibits.

We will start with examining 2D experiments with homogenous ECMs, using our model with the parameters μ_1 and μ_2 set to zero, considering a case with no proliferation of tumor cells and no renewal of the extracellular matrix molecules. After this, we will introduce proliferation and renewal, Incorporating μ_1 and μ_2 into the variation. Due to the immense computational effort, we will do a slimmer replication and parameter analysis for 3D experiments. After examining the model with a homogenous ECM initial condition, we will move on to a case considering a heterogenous ECM in 2D.

Looking at the parameter estimates from [2] to non-dimensionalise the time, we see that with $L \in [0.1cm, 1cm]$ and $D \approx 10^{-6} \frac{cm^2}{s}$, $\tau = \frac{L^2}{D}$ would give us a big temporal range, $\tau_{min} = 1000s$ and $\tau_{max} = 1000000s$ in which the simulations take place. However, using estimates taken from [11] and [5] for the length scale, with $L = 0.2cm$ gives us a concrete value for our non-dimensional time, $\tau = 40000s$, from now on t will stand as a replacement for τ for simplicity reason.

Since Anderson et al. do not specify the exact value for L , we needed to determine appropriate configurations for dt used in our simulation to get comparable results. We used a timestep of $dt = 0.01$, corresponding to $400s$, and let the simulations run for a dimensionless time of $t = 8$ corresponding to $320000s = 88 \text{ days}$. Looking at the results below, we found that for every unit of time in Anderson et al.'s experiments, in our experiments, $t = 0.4$ have passed.

Another challenge is diffusion and haptotaxis coefficients. Since they depend on the dimension we are in, we have to find our own estimates as a baseline value. The section regarding the 3D experiments with homogenous extracellular matrix structure has an extended discussion of this.

For each stage of the experiments, we will use a set of baseline parameters, which will be evaluated experimentally. From there, we will vary one or more parameters at a time

For all the plots of the experiments, the red curve indicates the tumor cell density, the blue curve the ECM density, and the green curve the MDE concentration. In all experiments, we used the value of $\epsilon = 0.01$ to match the initial conditions from [2] and [12].

4.1 2D Results without Proliferation and Renewal - Homogenous ECM

Every experiment in this section is done in two spatial dimensions. We define the initial conditions for the tumor cell density as:

$$c(x, 0) = \exp(\frac{-(x - 0.5)^2}{0.01})$$

$$m(x, 0) = 0.5c(x, 0) = 0.5 \exp(\frac{-(x - 0.5)^2}{0.01})$$
$$e(x, 0) = 1 - 0.5c(x, 0) = 1 - 0.5 \exp\left(\frac{-(x - 0.5)^2}{0.01}\right)$$

Figure 3 shows a 2D plot of the initial conditions using the homogenous extracellular matrix structure. The images describing the tumor cell density and the matrix-degrading enzyme concentration have high values in the center. The image describing the extracellular matrix has high values everywhere except the center since the matrix-degrading enzymes have already degraded the ECM.

[illegible]

Figure	Linestyle	d_c	γ	μ_1	η	μ_2	d_m	α	β
20 -right	——	$5 \cdot 10^{-4}$	0.0055	0	10	0	$1 \cdot 10^{-5}$	1.0	0.1
21 - left	$5 \cdot 10^{-4}$	0.0055	0	10	0	$1 \cdot 10^{-3}$	0.1	0.005
21 - left	——	$5 \cdot 10^{-4}$	0.0055	0	10	0	$1 \cdot 10^{-3}$	0.1	0.1
21 -right	$5 \cdot 10^{-4}$	0.0055	0	10	0	$1 \cdot 10^{-3}$	1.0	0.005
21 -right	——	$5 \cdot 10^{-4}$	0.0055	0	10	0	$1 \cdot 10^{-3}$	1.0	0.1

TABLE 1. Overview of all experiments conducted for the model without proliferation and renewal producing 2D output

Table 1 gives a detailed overview of all the experiments done in this section and the parameters used to produce the results. We are considering the model without the proliferation of the tumor cells or renewal of the extracellular matrix. Therefore, parameters μ_1 and μ_2 are set to zero. In most figures, more than one experiment will be described; the linestyle in table 1 determines which experiment exactly is described by the set of parameters.

4.1.1 Basecase Analysis

We will start with replicating the first experiment from Anderson et al.[2]. Figure 4 shows a screenshot of this experiment, unfortunately in low resolution, since the original paper had not included any digital data containing the diagrams of their results. In figure 4, you can see that after $t = 1$ in their timescale, the tumor cells develop a secession at the part invading the tissue. This secession propagates to a pointy peak at a later point in time. The concentration of the matrix-degrading enzymes increases continuously, and the concentration of the extracellular matrix decreases continuously. Their x -axis is stretched or rescaled to show an interval from 0 to 1. In our case, the interval on the plots has only x -values from 0 to 0.5. Replicating this experiment in two dimensions, we start with the same parameters as Anderson et al. had used, $d_c = 1 \cdot 10^{-3}$, $d_m = 1 \cdot 10^{-3}$, $\gamma = 0.005$, $\eta = 10$, $\alpha = 0.1$, $\beta = 0$. Figure 5 shows these results for four different points in time. The two-dimensional plots of the tumor cell density are shown on the left side, and on the right side, the plots produced by applying the Plot Over Line tool are displayed. As mentioned above, we will mostly resort to using only the results produced by the Plot Over Line tool. Figure 5 shows on the right side that the curves for the three variables are distinguishable, and we can estimate their values spacially and temporarily better than using 2D plots to estimate values.

Starting from the initial values, we see that after $t = 4$, a very small secession of the tumor cells is starting to form. This secession increases in the image at $t = 4$, but at $t = 8$, it has visibly flattened. This secession is not as pointy as seen in the one-dimensional experiments. The interplay of the diffusion and haptotaxis factors determines how considerable this secession will be that splits from the primary lump of the tumor cells and invades the tissue faster. It will also decide how pointy this secondary lump of tumor cells will be. Biologically, this relation between diffusion and haptotaxis translates to the invasion pace of the tumor cells, the rate at which much of them will remain at the center, and how much will invade further into the tissue.

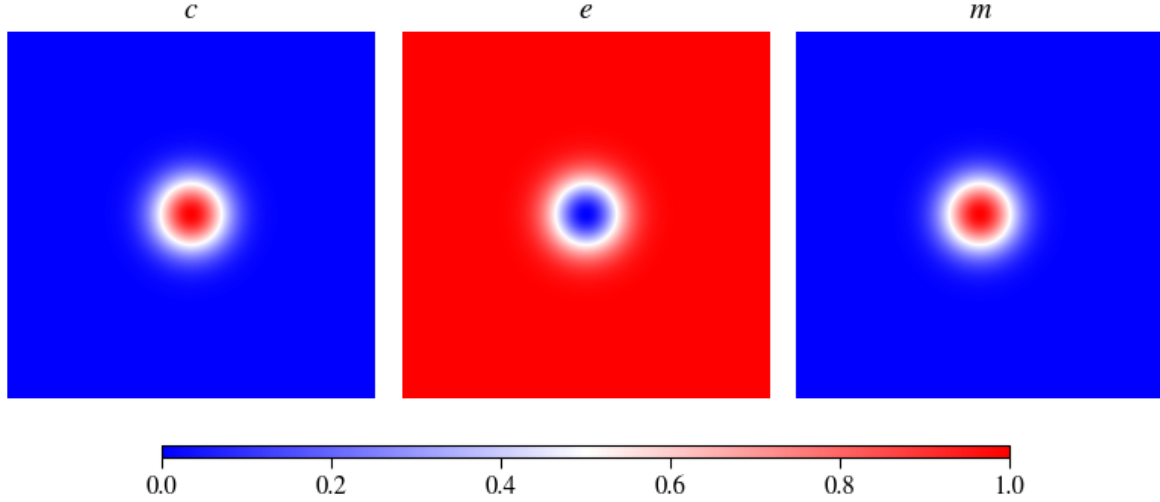


FIGURE 3. Visualization of the initial value distribution for an experiment in two space dimensions with a homogenous extracellular matrix

Looking at the concentration of matrix-degrading enzymes, we see it is visibly lower here than in Anderson et al.'s experiment. We see little increase across time. We can change this by changing the production factor of α . This factor determines how fast the tumor cells produce the matrix-degrading enzymes, degrading the extracellular matrix and allowing the tumor cells to invade the tissue further.

Only the extracellular matrix concentration seems to mimic the behavior of Anderson et al.'s experiment. It decreases continuously, and as the last image shows, there is still a considerable amount left.

To replicate Anderson et al.'s results, we will start adjusting the parameters mentioned: the tumor cells' diffusion coefficient, their haptotactic coefficient, and the production rate of the matrix-degrading enzymes. Making the curves fit ideally will be impossible due to the system's high degrees of freedom and the change of dimension. Regardless, we will replicate as best as possible, focusing on the values the variables will take at the origin $x = 0$.

Starting with comparing different values for α , we see in figure 6 a comparison of how this affects the curve for the matrix-degrading enzyme concentration. A maximum difference between the compared values of 0.2 already causes drastic changes. In Anderson et al.'s experiment, we observed a value of approximately $m(0, 1) = 0.5$ after, in their timescale, $t = 1$ at the origin. This value is mimicked best for a value of $\alpha = 0.2$ in our experiments. However, in the later points in time, we see that this value for α is insufficiently low in terms of increase, though choosing α higher than $\alpha = 0.4$ results in an accelerated ECM degradation that is too fast. Taking a value between those two allowed our simulations to exhibit the observed behavior. We choose a value of $\alpha = 0.35645$ to use in the later experiments as a basecase.

Looking at the diffusion coefficient for the tumor cells, in figure 7, you can see different

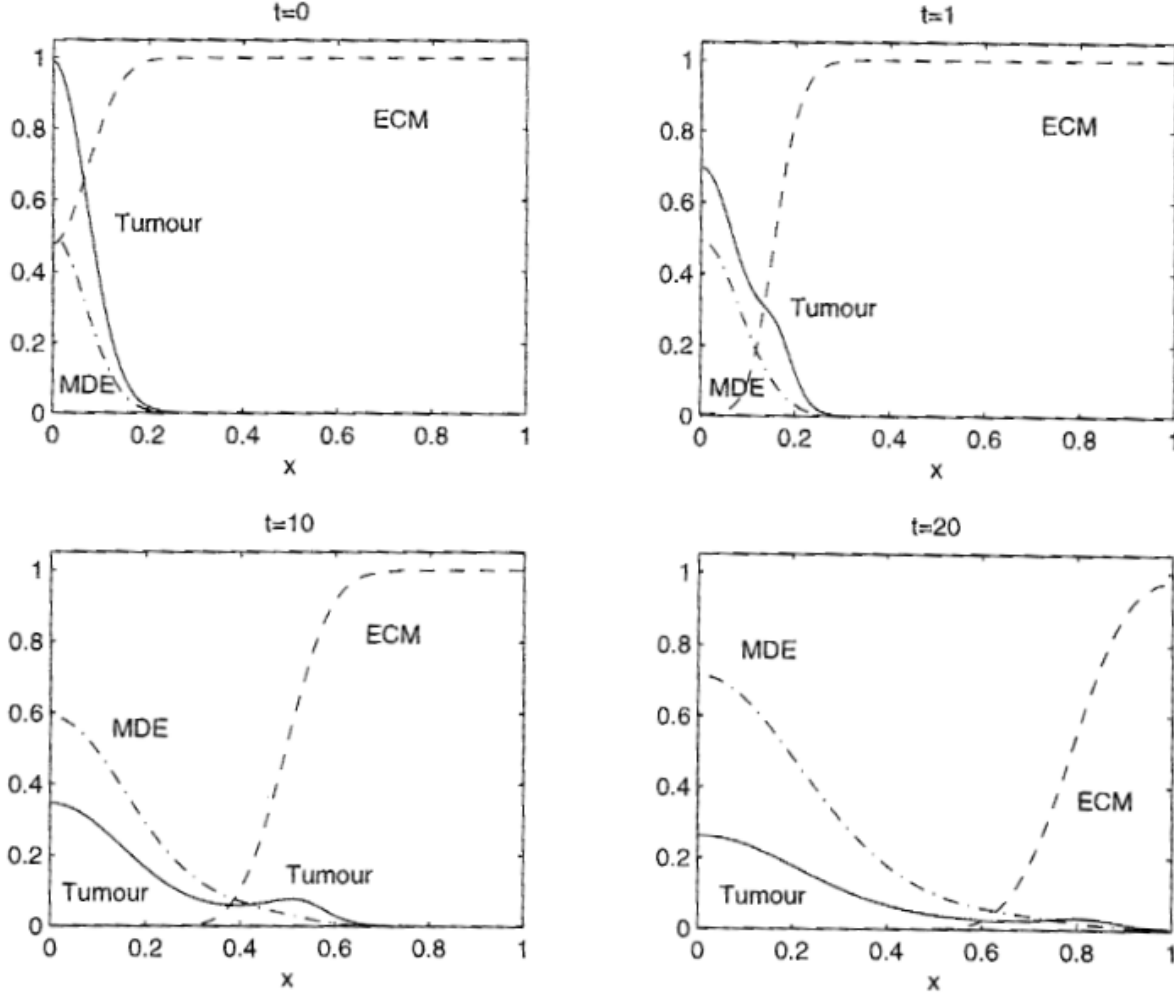


FIGURE 4. Andersons first one dimensional experiment using the parameter values $d_c = 1 \cdot 10^{-3}$, $d_m = 1 \cdot 10^{-3}$, $\gamma = 0.005$, $\eta = 10$, $\alpha = 0.1$, $\beta = 0$, $\mu_1 = 0$, $\mu_2 = 0$

d_c values regarding the tumor cell concentration. It is clear that with decreasing d_c , the sharpness of the secondary lump of cells that begins to invade the tissue drastically increases due to increased effects of haptotaxis, which is now the main factor in controlling tumor motility. However, we also observe that with decreasing d_c , the remaining lump of tumor cells at the origin increases due to little diffusion here. Over time, we found that $d_c = 5 \cdot 10^{-4}$ describes Anderson et al.'s experimental results best for our simulations, with a roughly matching density of tumor cells that remains at the origin at all times and, for our case, balanced effects of haptotaxis and diffusion.

At last, we want to adjust the haptotactic pull slightly; for this, we are looking at a comparison of different γ values in figure 8 depicting the tumor cell density. Comparing our results with Anderson et al.'s, we want a bigger secondary lump that invades the tumor cells faster than the one remaining at the origin. We need to increase γ to increase the haptotactic pull that controls tumor cell motility. The figure shows that increasing γ yields these effects, but increasing it too much results in a too-fast invasion pace of the

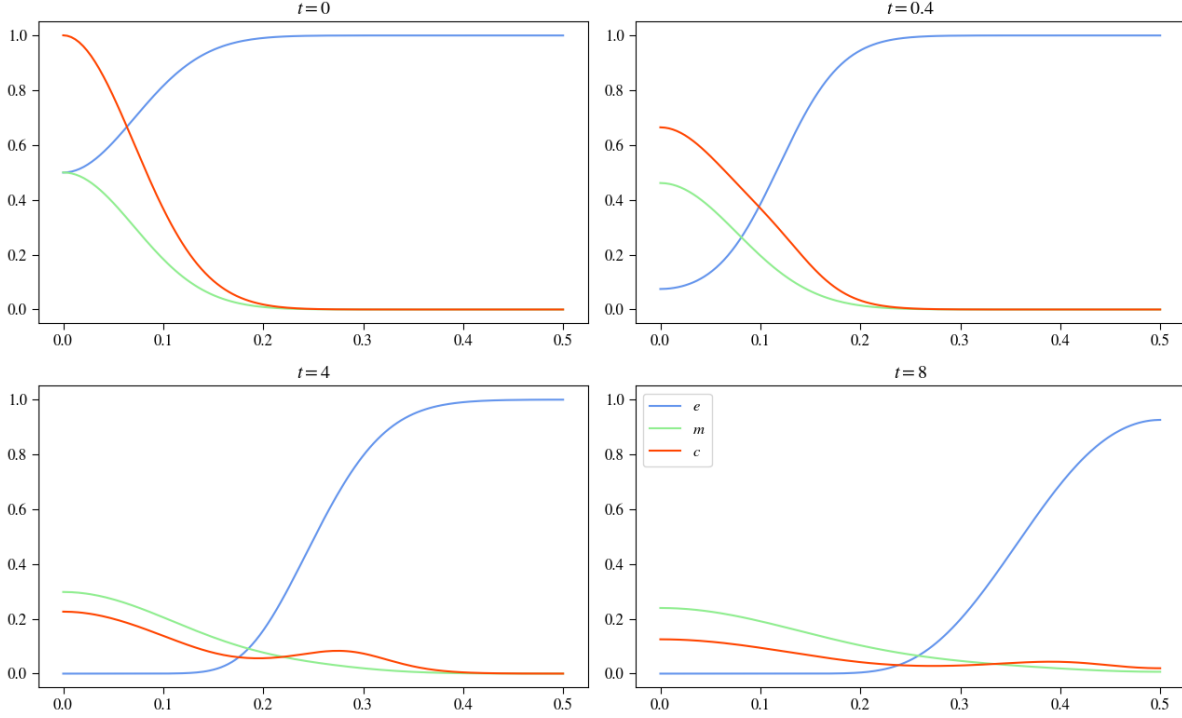


FIGURE 5. Results using Anderson et al.'s parameters produced by applying the Plot Over Line tool

surrounding tissue. Increasing γ slightly to $\gamma = 0.0055$ is sufficient to produce the desired effects.

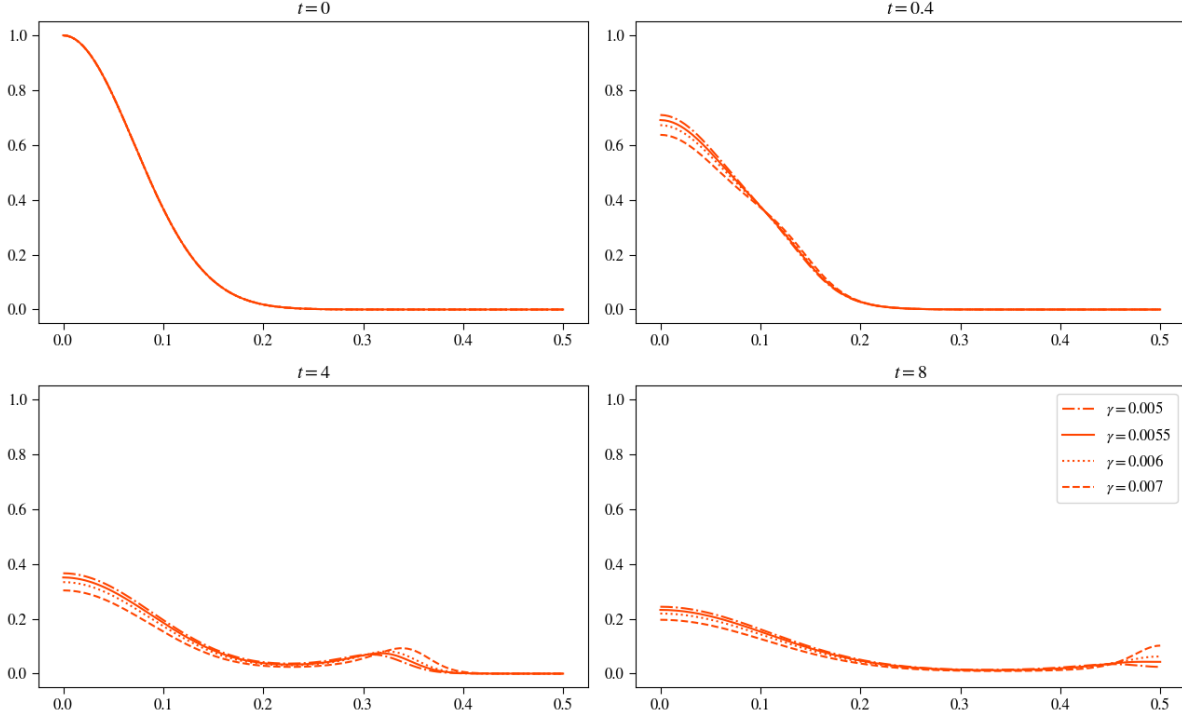
These adjustments leave us with the final configuration for replicating the system with the curves in figure 9 and the parameter settings of $d_c = 5 \cdot 10^{-4}$, $\gamma = 0.0055$, $\eta = 10$, $d_m = 1 \cdot 10^{-3}$, $\alpha = 0.35645$, $\beta = 0$. We see the important effects met when comparing our final version with the original experiment we are trying to replicate, figure 4. We see that the production of the matrix-degrading enzymes fits the original experiment, and the motility of the tumor cells also matches, with balanced effects of haptotaxis and diffusion.

4.1.2 Parameter Analysis

Before we start with the parameter analysis, we will discuss the mathematical intuition concerning the system of partial differential equations, equations 6 to 10.

The equation governing the tumor cell density incorporates only two coefficients in this version regarding its motility, diffusion, and haptotaxis. As mentioned during replicating Anderson et al.'s experiment, the relation between those two factors determines if a secondary lump of tumor cells secedes itself from the main lump and invades the tissue faster than the remaining cells but also how large this lump will be. We saw this behaviour in figure 7, varying d_c whilst keeping γ constant. Diffusive motility depends on the laplacian of the tumor cells themselves, $\Delta c = \frac{\partial c}{\partial x} + \frac{\partial c}{\partial y} + \frac{\partial c}{\partial z}$, which is a fundamental tool in sciences of all sorts to describe the effects of spacial rate of change of a scalar field quantity, in

FIGURE 6. Comparison of α values to replicate Anderson et al's experimentFIGURE 7. Comparison of d_c values to replicate Anderson et al.'s experiment

FIGURE 8. Comparison of γ values to replicate Anderson et al's experiment

our case tumor cell density, at a specific point in space. Typically, this operator has high values where the respective quantity changes rapidly. We have a similar haptotaxis term: $\nabla \cdot (c \nabla e) = \nabla c \cdot \nabla e + \Delta e$. This relation means that haptotactic effects are strong not only where the concentration of the extracellular matrix changes rapidly but also where both gradients for tumor cell density and extracellular matrix assimilate in direction. However, these effects can also annihilate each other.

The equation describing the concentration of the extracellular matrix models its exponential decay, taking the concentration of the matrix-degrading enzymes into account. In spatial and temporal positions where both ECM and MDE concentrations are high, we can expect a fast degradation of the extracellular matrix.

The equation modeling the matrix-degrading enzymes combines motility with production/decay terms. The motility of the MDEs is modeled by the same diffusion as the tumor cells, mimicking their behavior in this regard. The tumor cells are responsible for producing the MDEs; the production is modeled by natural decay, and both production and decay are modeled using exponential approaches.

From the replicated results shown in figures 9, we saw that the results can vary strongly if we vary the parameters one at a time. We will first look at how changing one parameter at a time affects the output of the simulation. After this, we will consider changing multiple parameters simultaneously in the cross-variation section. For varying the parameters, we assume the other parameters of the system are constant and use the baseline experiment as their values.

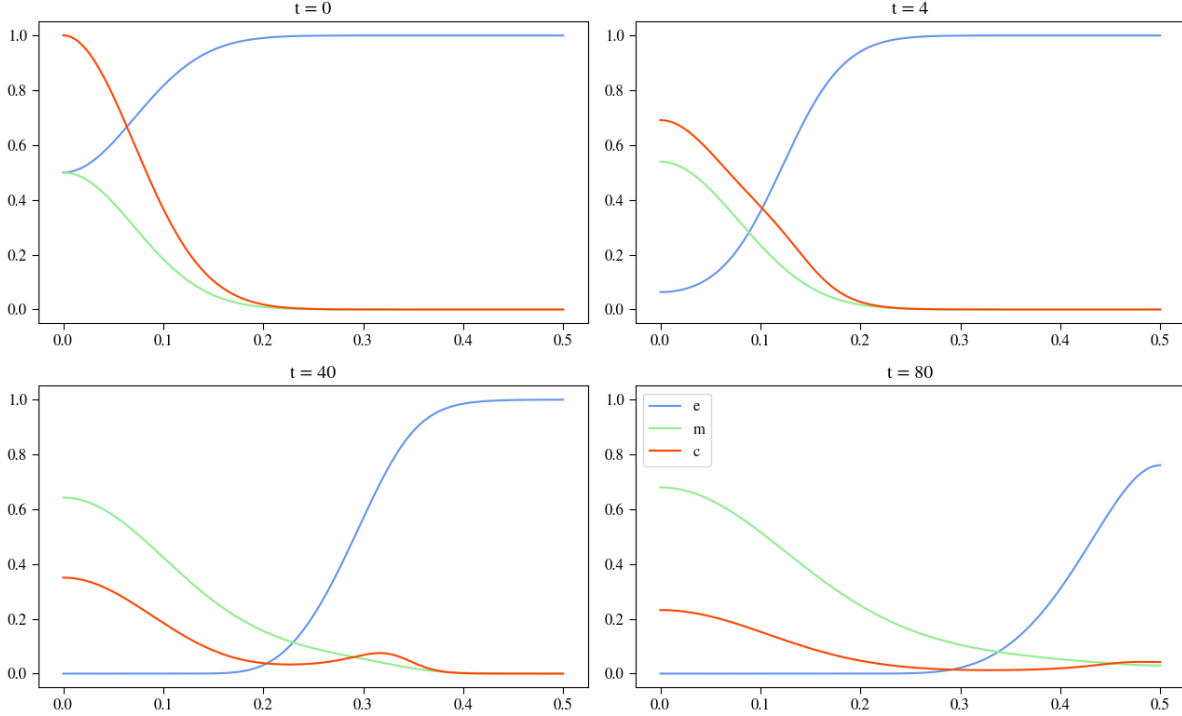


FIGURE 9. Results of using the parameters as described, this experiment will be used as the basecase to compare further experiments regarding the model without proliferation and renewal

d_c Variation

This parameter describes the diffusive properties of the tumor cells. As Chaplain et al. assumed in [11], we are also assuming an even distribution of this parameter with $d_c \sim U[1 \cdot 10^{-5}, 1 \cdot 10^{-3}]$. However, our experiments encountered numerical instabilities reducing the parameter further than $5 \cdot 10^{-5}$.

As described, the intuition is that decreasing d_c will increase the effects of haptotaxis and make γ more influential. This means the tumor cells will drift faster outward with a bigger secondary lump, forming a pointier leading edge. On the other hand, if we increase d_c , the effects of haptotaxis will diminish, and the tumor cells will be subject to higher diffusion, distributing them more evenly in the tissue. Additionally, there will be less secession from the primary lump of cells. Looking at the experiments in figure 10, we can see these assumptions met. The smaller d_c gets, the higher the influence of haptotaxis; therefore, γ will be and vice versa.

Considering the tumor cell density curves shown in red, we can see minor differences after already $t = 0.4$. For the two lower values of d_c , the solid and dashed curves, we see the tumor cells having a higher concentration at the origin than for the biggest value of d_c , dotted curve, nearly overlaying each other. The red dashed curve is considerably lower at the origin, though it is stretched out more than the other two, indicating a faster invasion rate. The other curves describing EDM and MDE concentration do not show any deviations from each other at this point.

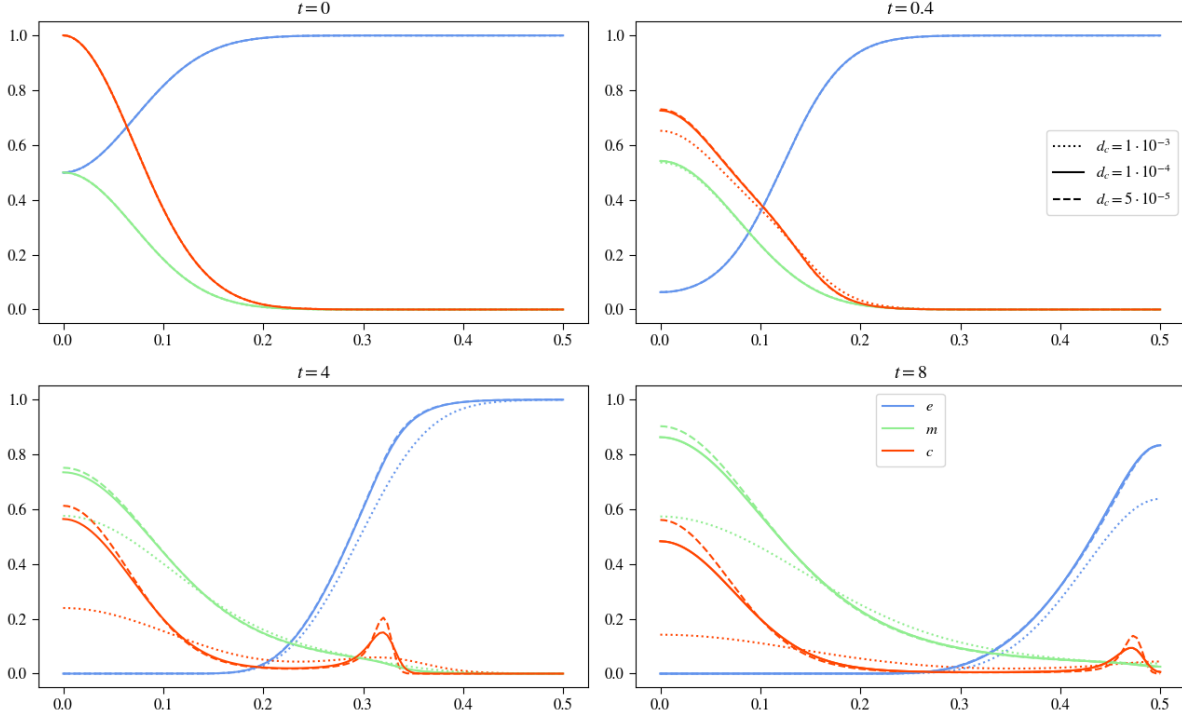


FIGURE 10. Results of varying d_c in the basecase parameter set, keeping the other parameters constant, using the Plot Over Line tool

Looking at the plot results, at time $t = 4$, we see the previously observed effects increase. The curves of the tumor cells confirm that with increasing d_c , the remaining lump of cells at the origin decreases, distributing the tumor cells more evenly in space and also reducing the effect of haptotaxis, making the secondary lump, which is still visible for the highest diffusion term, less sharp. At this point, the other two curves also show differentiating behavior. The ECM is degraded faster with increasing d_c , and the slope the ECM describes is less steep. Looking at the extracellular matrix, we see minor differences between the lower two values for d_c . Due to the tumor cells' exponential production of the MDEs and the more even spread of the tumor cells, we see them taking on a lower concentration at the origin. However, we can also observe that they have spread farther out than the MDE concentrations describing the experiments with lower d_c values.

Studying the last image of $t = 8$, we see no new effects, only the already mentioned propagated; with increasing d_c , we see a more even spread of the tumor cells and a reduction of the secondary lump, leading to the invasion of the tissue. For the MDE concentration, we observe less concentration in total due to the exponential growth rate, especially at the origin. However, we also see a more even distribution of them and a slightly faster invasion pace. This causes the extracellular matrix degradation to work faster.

Regarding the sensitivity of this parameter, the higher the value is, the more sensitive the system reacts. Though the lower two values for d_c are only separated by $5 \cdot 10^{-5}$, and we can unfortunately not experiment with $d_c = 1 \cdot 10^{-5}$ due to numerical instabilities,

the differences between those two were minimal compared to the difference between the higher two values of d_c .

From a biological point of view, this increase in diffusion might be caused by a change in temperature, electric potential, or mechanical pressure differences. The higher diffusion results in a more even spread of the two actively moving quantities of tumor cells and matrix-degrading enzymes, which degrade their surrounding tissue, the ECM, at a faster rate.

γ Variation

γ describes the effects of haptotaxis; it is assumed that it is evenly distributed in $\gamma \sim U[0.001, 0.01]$, like Anderson et al. [2] assumed. Like Anderson et al., we will also look at values exceeding this region, though most likely losing their biological meaning. Inspecting the effects of γ , we can assume the countering effects on the tumor cells as for varying d_c ; selecting higher values for γ will increase the effects of haptotaxis, creating a larger secondary lump of cells that is being pulled faster into the tissue. The experiments

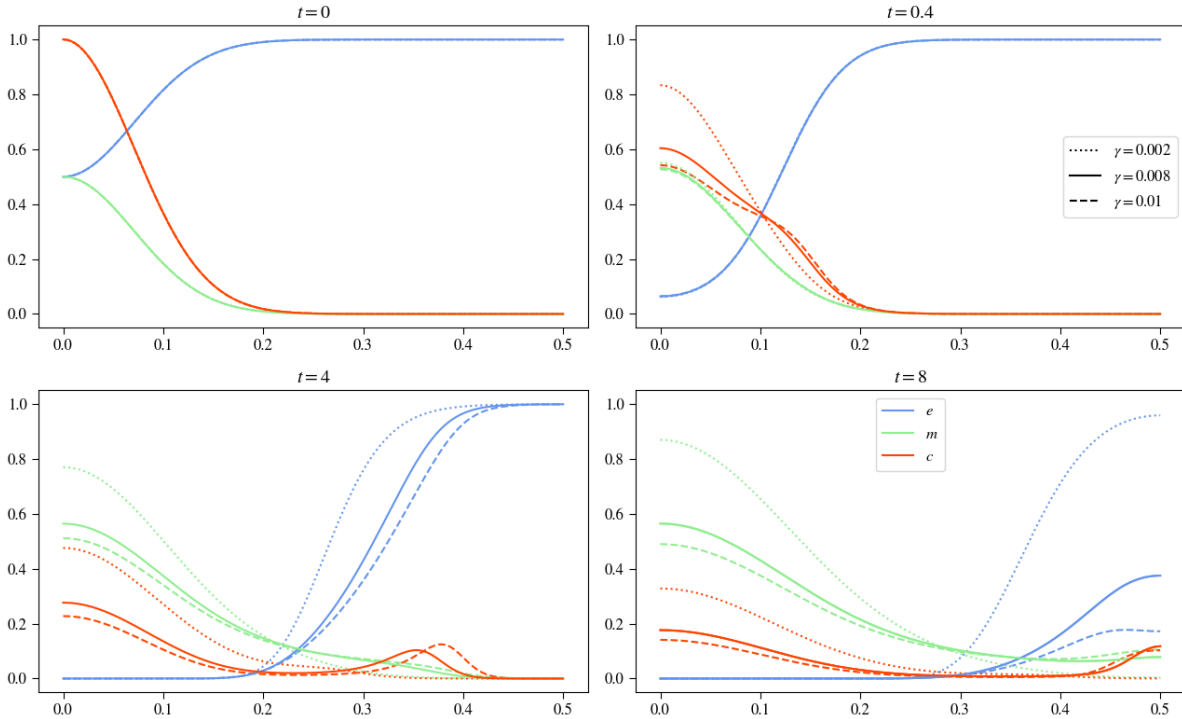


FIGURE 11. Results of varying γ in the basecase parameter set, keeping the other parameters constant, using the Plot Over Line tool

described in figure 11 verify the expected behavior.

After $t = 0.4$, we already see apparent changes for varying γ ; the higher γ is set, the more secession for the tumor cells is observable, which will later form the secondary lump. The lowest value for γ , undercutting the one for the basecase, shows no signs of a leading edge forming that invades the tissue separately. The two higher values for γ show little

deviation. Considering the other two variables, extracellular matrix concentration and matrix-degrading enzyme concentration, no change is visible, still overlaying each other at this temporal point.

The following image shows the simulation after $t = 4$ timesteps; we can see changes in all three variables. While the tumor cell density for the values of 0.008 and 0.01 differ slightly by the number of cells that are left at the origin and the distance they have already invaded the surrounding tissue, the curve for the lowest γ value, as at $t = 0.4$ does not show a secession of the tumor cells that invades the tissue separately, which causes the tumor cells to stay centered around $x = 0$, resulting in a higher density of cells there compared to the results of the other experiments. With increasing γ , the invasion speed also increases, as the dashed line for the tumor cell density shows. For the MDE curve, we also observe that the lower γ is, the more concentration is at the origin due to the higher remaining density of tumor cells at the origin. The ECM concentration shows behavior similar to the MDE concentration; with increasing γ , the ECM is faster and more evenly degraded; due to the faster invasion of the tissue, the production of matrix-degrading enzymes also happens in regions farther away from the center. As we saw varying d_c , only a little MDE concentration is needed to degrade the extracellular matrix efficiently. Therefore, the ECM degradation process also happens faster here.

In the last image at $t = 8$, we see the observations from previous points in time confirmed; the higher γ , the faster the invasion pace of the tumor cells and the more secession forms with fewer tumor cells staying at the origin. The behavior of the tumor cells causes a higher concentration of MDEs at the origin due to exponential growth and a steeper decline moving outwards. With rising γ , the ECM is getting degraded faster.

Out of curiosity, we will take a step further and increase γ again by one power to $\gamma = 0.1$. As previously observed, the haptotactic effects of pulling the cells into surrounding tissue increase, causing an even faster invasion pace. However, in this case, the invasion pace of the tumor cells is so high that no cells are left at the origin; everything is being pulled into the surrounding tissue. Before finishing the simulation after $t = 8$, the tumor cells have reached the domain Ω 's border. The cells are being reflected at the border due to the boundary conditions of our model 9 and 10. In figure 12, you can see that after $t = 2$, the border is reached, and at $t = 3$, the cells have been reflected to move into the corners, where the ECM concentration is highest. At $t = 3$, the pace of the ECM degradation of the matrix-degrading enzymes has not been able to keep up with the invasion pace of the tumor cells. After being pulled into the corners at $t = 3$ and degrading the ECM there, at $t = 6$, the tumor cells are being pulled back toward the center of the simulation.

Though this behavior matters little from a biological perspective due to the system's boundary conditions reflecting the movement and high invasion pace of the tumor cells, it is still interesting to investigate this case from a numerical perspective.

Though the intuition is met that with increasing γ , the invasion pace of the tumor cells and matrix-degrading enzymes also rises, we get unexpected behavior in the last experiment. There is more of a total ECM concentration left than in the experiment using $\gamma = 0.01$. Studying those experiments biologically, we know that the term extracellular matrix describes a whole class of different molecules, minerals, or proteins, like collagens

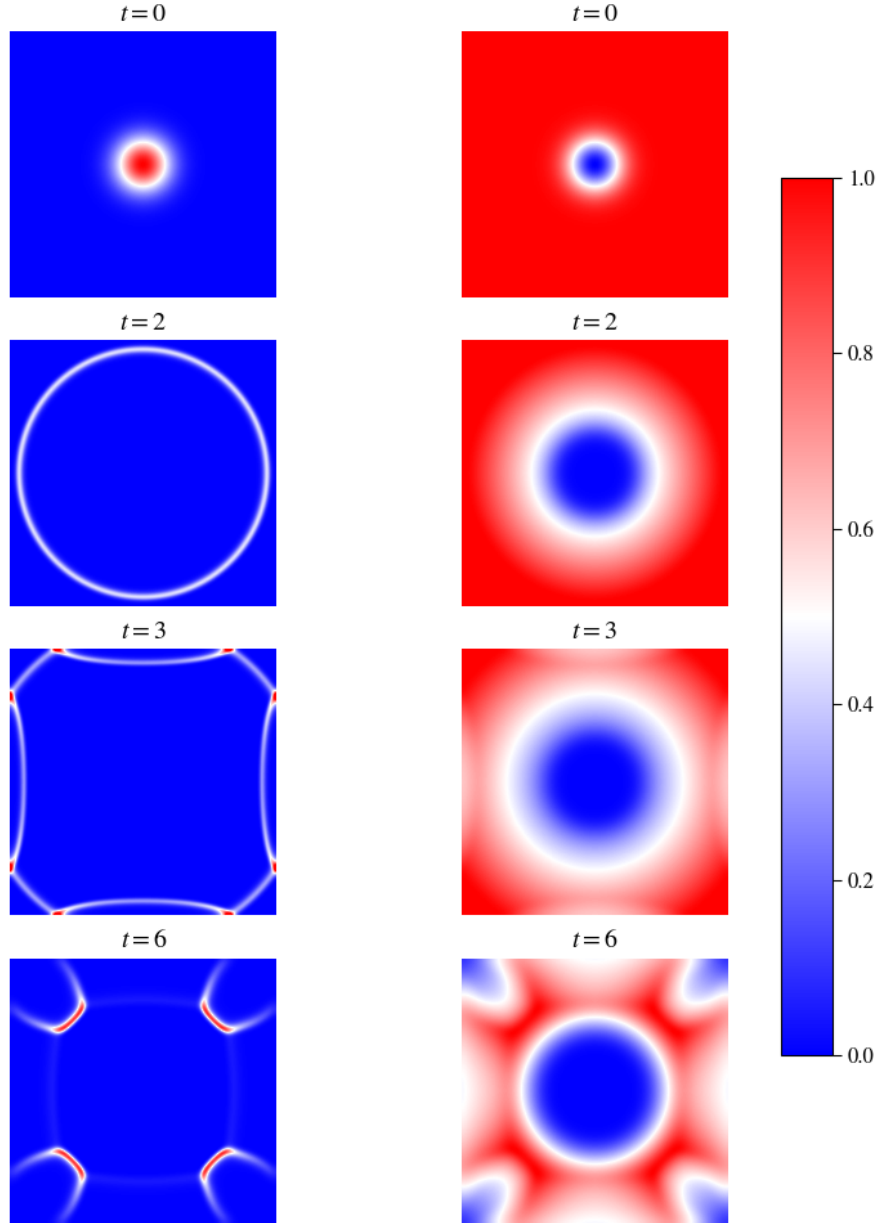


FIGURE 12. 2D plot showing experiment for $\gamma = 0.1$, left tumor cell density, right ECM concentration

or enzymes. The different properties of these elements cause varying effects of haptotaxis. For example, were the haptotactic effects measured on laminin considerably lower than then ones measured on fibronectin, according to Aznavoorian et al. [13]. Different constellations of extracellular matrix composition will be encountered in different human body sites, which will cause the tumor cells, as seen in the numerical experiments, to behave differently.

η Variation

The parameter η controls the degradation process of the extracellular matrix molecules. Since Anderson et al. [2] used a value of $\eta = 10$ on all their experiments, we assumed an even distribution in $\eta \sim U[0, 20]$. The degradation process of the extracellular matrix is modeled using an exponential decay hypothesis, so we can expect that increasing η also increases the system's sensitivity concerning the parameter η . With its role in controlling the degradation, it will also heavily influence the motility of the tumor cells and, therefore, the motility and production rate of the matrix-degrading enzymes. Slower degradation will result in a higher density of tumor cells at the origin, exponentially producing matrix-degrading enzymes. This, in turn, will increase the ECM degradation. With increasing η , the ECM is faster degraded and, therefore, might provoke a faster invasion rate of the tumor cells of the surrounding tissue. The higher η is, the fewer MDEs are needed to degrade the ECM efficiently.

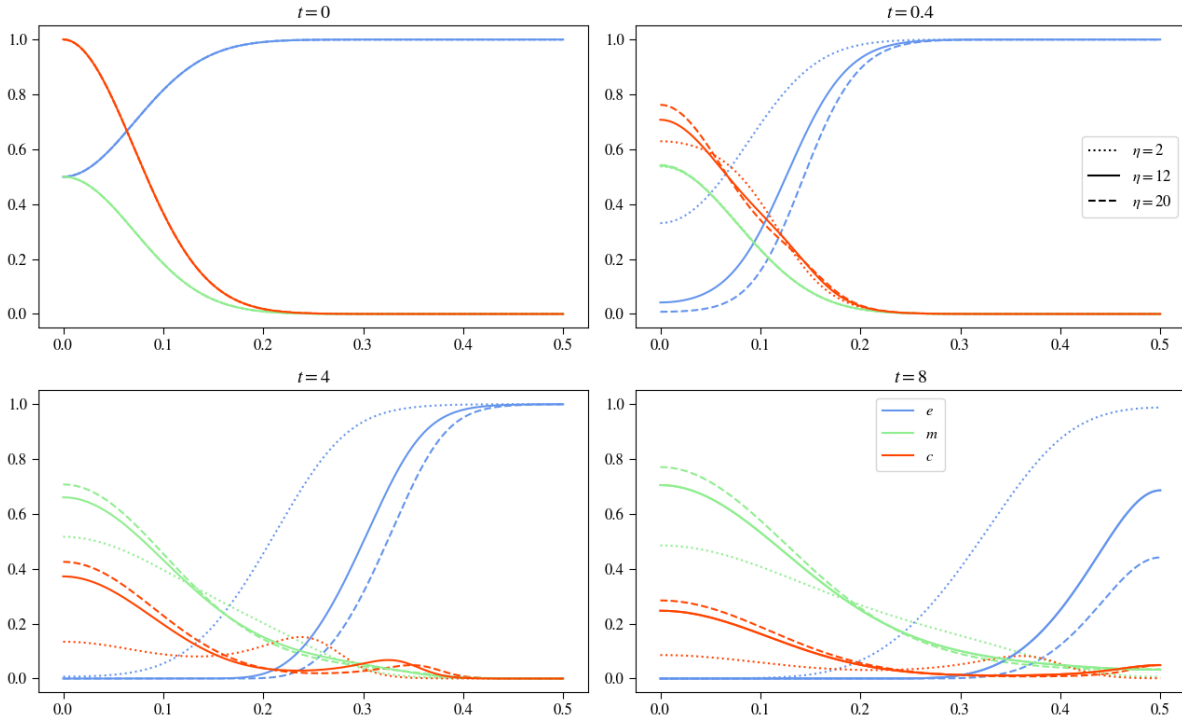


FIGURE 13. Plots show results for varying η while keeping the other parameters constant; in the images you can see the effects of $\eta = 20$ in the dashed curve, $\eta = 0$ in the dotted curve, and $\eta = 12$ in the solid line.

Inspecting the results in figure 13, it is most striking that the slower degradation rate causes a slower tumor invasion.

We see significant differences for both curves, tumor cell density, and ECM concentration after $t = 4$. Inspecting the experiment with $\eta = 2$, we see that the ECM has only degraded a little, exposing the tumor cells to stronger haptotactic pull by the ECM in regions closer to zero, compared to the other experiments. Though it may look like

no secondary lump of cells is being formed, the contrary is the case; even more cells are pulled into the tissue, with the ECM slowly receding into the tissue, which smooths out the bump the other two curves show for the tumor cell density. This results in only one lump of tumor cells that invades the tissue without one remaining at the origin. The same effect is observable when comparing the tumor cell density curves for the higher η values. With fewer tumor cells pulled by the ECM, the higher η gets. Only the curve for the matrix-degrading enzymes has not been affected by the variation of η until now.

The next image at $t = 4$ propagates the effects on the tumor cells and the ECM. The slower the degradation process, the more tumor cells invade the tissue, and the less of a secession is observable. The movement now also affects the concentration of the matrix-degrading enzymes. With the fewer remaining tumor cells at the origin producing the MDEs, we also see a more minor concentration at the origin. However, the distribution of the tumor cells for the lowest case of varying η has a more even distribution of MDEs.

The same goes for the last image, showing the experiments at $t = 8$. The more even the distribution of tumor cells and matrix-degrading enzymes across space, the slower the ECM is degraded.

As mentioned, varying γ does the term extracellular matrix include various organic or inorganic compounds. Therefore, the build-up and properties of these compounds vary strongly and motivate this comparison of degradation rate. Some compounds may be degraded faster, while others are complex and need more time to degrade.

d_m Variation

d_m describes the diffusion coefficient for the matrix-degrading enzymes. As estimates, we use Anderson et al.'s and Franssen et al.'s, which assume an even distribution of d_m in $\sim U[1 \cdot 10^{-5}, 1 \cdot 10^{-3}]$. Having set $\beta = 0$, equation 8 modeling the temporal development of the matrix-degrading enzymes concentration only depends on c concerning motility as well as in production. As we saw in experiments before, we can expect a high concentration of MDEs in regions with a high density of tumor cells, and we can expect increased motility where the density of the tumor cells rapidly changes. Increasing d_m will cause a faster, more even spread of the MDEs in the surrounding area, and therefore, the ECM will also be degraded faster.

Inspecting the results in figure 14, we observe that in the second image after $t = 0.4$, the curves of the tumor cell density and the ECM are mostly untouched, though looking closely, we can see that for the highest d_m value, dotted line, the ECM has at the origin higher and farther out lower concentrations of the ECM. This is caused by the more even distribution of the matrix-degrading enzymes, which visibly reduce the concentration at the origin and invade the surrounding tissue slightly faster at this point.

The following image shows the experiments after $t = 4$, and we see the differences between the lowest d_m value experiment with the other two more pregnant. The MDE concentration has, relative to the other two, strongly decreased at the origin, though it has invaded the tissue further. The ECM has degraded faster, and as we saw in the η variation, the faster ECM degradation reduces the effects of haptotaxis. The other two experiments differ only visibly regarding the MDE concentration, though it exceeds

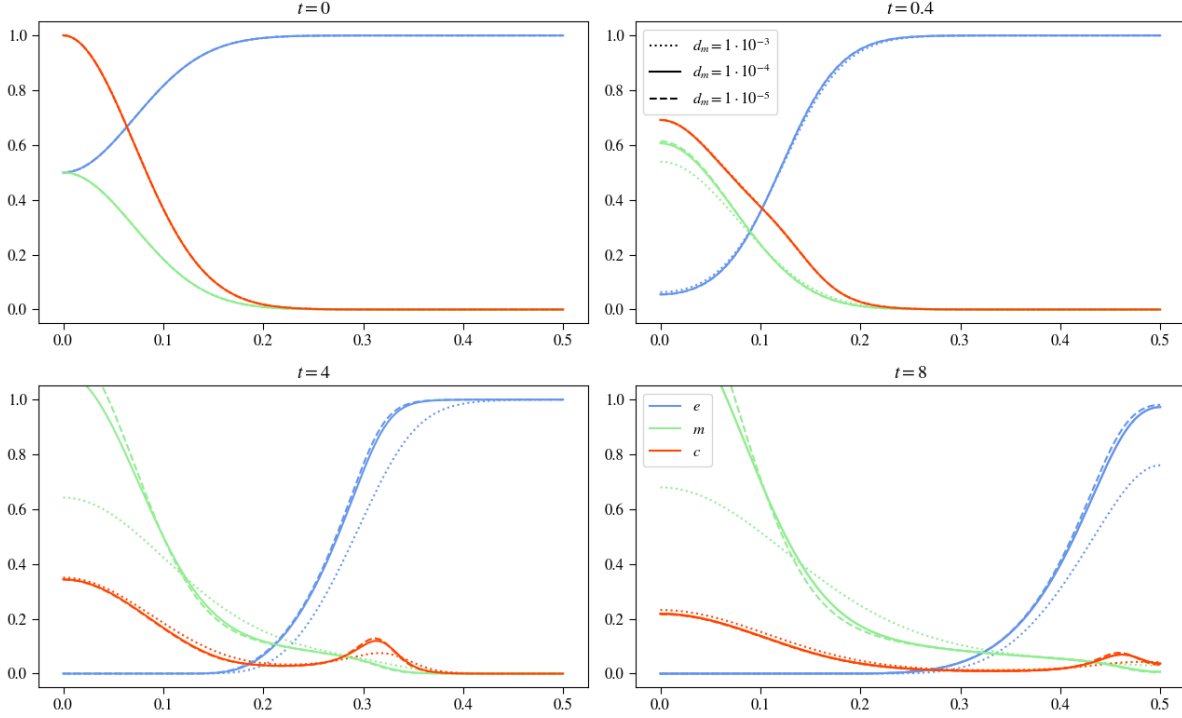


FIGURE 14. Plots show results for varying d_m while keeping the other parameters constant; in the images you can see the effects of $d_m = 0.1$ in the dashed curve, $d_m = 0$ in the dotted curve and $d_m = 1 \cdot 10^{-3}$ in the solid line.

the limits of the plot. The concentration at the origin for the lowest diffusive value is considerably higher than for the middle value.

The last image confirms the abovementioned effects, with the most substantial deviations between the highest d_m experiment and the other two. Again, a more even spread of the MDEs with a lower concentration at the origin, a faster ECM degradation, and tumor cell density curves that, compared to the other experiments, have less secession at its leading edge. The two experiments with lower d_m values still have nearly overlaying tumor cell density and ECM curves. Only the MDE concentration differs between the two, showing a more even spread for the higher diffusion value, though with a lower value at the origin.

Seeing those effects, we saw our intuition met, though it is to say that looking at the lower two values for d_m , the differences here were modest. Therefore, the higher the value for d_m is, the more sensitive the system reacts to this change.

These changes in diffusion, like in the section varying the diffusion coefficient of the tumor cells, might be caused by a multitude of physical influences, such as temperature, voltage, pressure, etc. The results show that this change causes a faster degradation of the extracellular matrix molecules but a less aggressive invasion of the tumor cells.

α Variation

The parameter α influences how fast the tumor cells produce matrix-degrading enzymes. We assume it to be evenly distributed with $\alpha \sim U[0, 1.0]$ since Anderson et al. assumed the same range in the original paper. Trying to replicate Anderson et al.'s experiment, we already saw how varying α affects the simulation results. With growing α , we will see a higher concentration of MDEs, especially in regions with high tumor cell density. More MDEs will cause faster degradation of the ECM first due to having more of them, but also because since more of them are subject to diffusion, they will spread faster in the tissue. Faster ECM degrading could mean an increased invasion pace of the tumor cells. As we saw in the previous experiments varying d_c , the MDE concentration can take on values higher than one. We can also expect this here when α is sufficiently high.

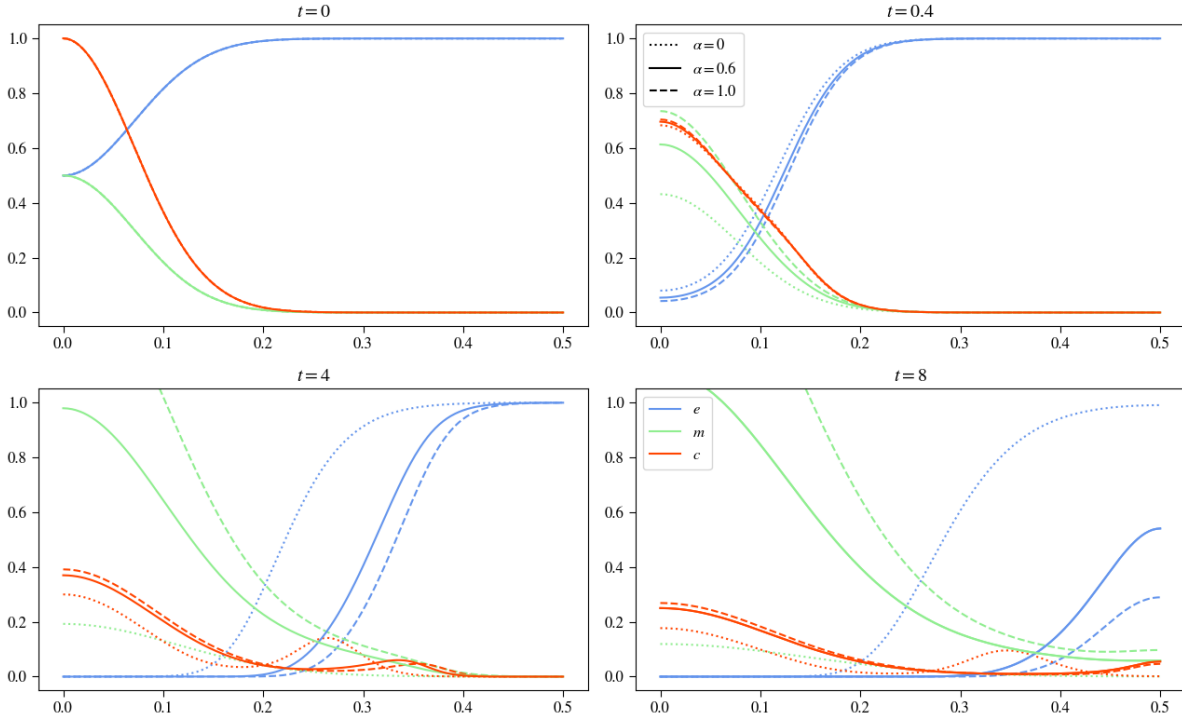


FIGURE 15. Plots show results for varying α while keeping the other parameters constant; in the images, you can see the effects of $\alpha = 1.0$ in the dashed curve, $\alpha = 0$ in the dotted curve, and $\alpha = 0.6$ in the solid line.

The second image of figure 15 describes the experiments after $t = 0.4$. We can clearly see the differences in the MDE curves for the different values of α . The other curves also show slight deviations. The higher α is, the faster the ECM degradation. Looking closely, we can observe for the tumor cell density that the increased rate of ECM degradation results, as previously already seen, in a curve with less of a bump that will later form the secession invading the surrounding tissue due to more minor haptotactic influences at the origin.

The next point in time, at $t = 4$, shows the previously mentioned effects in a reinforced

way. For $\alpha = 0$, the MDEs have no producing factor, and the curve flattens due to diffusion, though the extracellular matrix has degraded visibly, yet at a considerably slower rate. This experiment has the lowest density of tumor cells at the origin, though the most significant secondary lump of cells invades the tissue. This behavior is due to the extended exposition of strong haptotactic influences near the origin region, which pulls more cells outward to invade. The solid curves describing $\alpha = 0.6$ show that at this point, they have almost reached a concentration of one at the center, which will be exceeded later. Compared to the lowest α experiment, the faster ECM concentration has also pulled less of the tumor cells outward, though at a faster invasion pace. Looking at the experiment with the highest α value, the MDE concentration already exceeds one, the ECM degradation is happening faster, and the invasion of the tumor cells is happening faster, though with a lower density.

In the last timestep, we see that the MDE curve of $\alpha = 0.6$ and $\alpha = 1.0$ exceeded one. For the dotted curve of the MDE, we have a good example of diffusion distributing the concentration throughout space without changing its overall volume. At the border regions, we see that the dotted curve is also the only one that has yet to degrade any ECM in this area, while the other two experiments show that there is only a little ECM concentration left to degrade. The tumor cells confirm the, in the previous timestep mentioned, effects of faster invasion pace with rising α though with at a thinner density.

Our initial assumptions were correct with a faster degradation pace due to higher MDE concentration and, therefore, a faster invasion pace of the tumor cells. However, it is interesting to see that the more minor α , the more tumor cells are being pulled into the tissue.

While it makes sense from a numerical perspective that the concentration of MDEs can exceed one, it might make sense to introduce a finer grid or adapt the model in other ways since, judging from a continuous perspective, it does not make sense that at a certain point in space, there is more than one entity occupying this space.

The production of matrix-degrading enzymes can have many biological causes. During many natural processes like tissue repair or remodeling, the extracellular matrix must be degraded, controlled by cells producing enzymes that, in turn, are responsible for producing matrix-degrading enzymes. This control flow can be interrupted by malignant cells stimulating the production of MDEs without any repair or remodeling tasks to perform. Considering the absence of or reduced MDE production, we can regard this case as the consequence of a drug treatment. On the other hand, since there are plenty of different extracellular matrix molecules, they may also have different production rates.

β Variation

The factor β controls the decay of the matrix-degrading enzymes, and the results of its variation are shown in figure 16. Using Kolev et al.'s estimate for β in [12], we experimented with $\beta = 0.07$. Considering the results, we can assume an even distribution of β in $\beta \sim U[0.005, 0.1]$. Interestingly, α and β are their respective distribution, and the experiments will confirm that they are not of the same magnitude. While the MDEs are produced by the tumor cells, their decay is controlled by the MDEs themselves. This model assumes that the tumor cells do not proliferate, which makes their total amount

constant. In contrast, the MDEs are produced by the tumor cells and are expected to change in amount over time due to production or decay. This makes the decay rate of the MDEs more variable because of the changing amount of total MDEs, causing the change of effective magnitude.

With introducing β foremost, we can assume that the MDE curve will be lower, influencing the ECM degrading process and, therefore, the invasion pace and the diffusion-haptotaxis effects on the tumor cells.

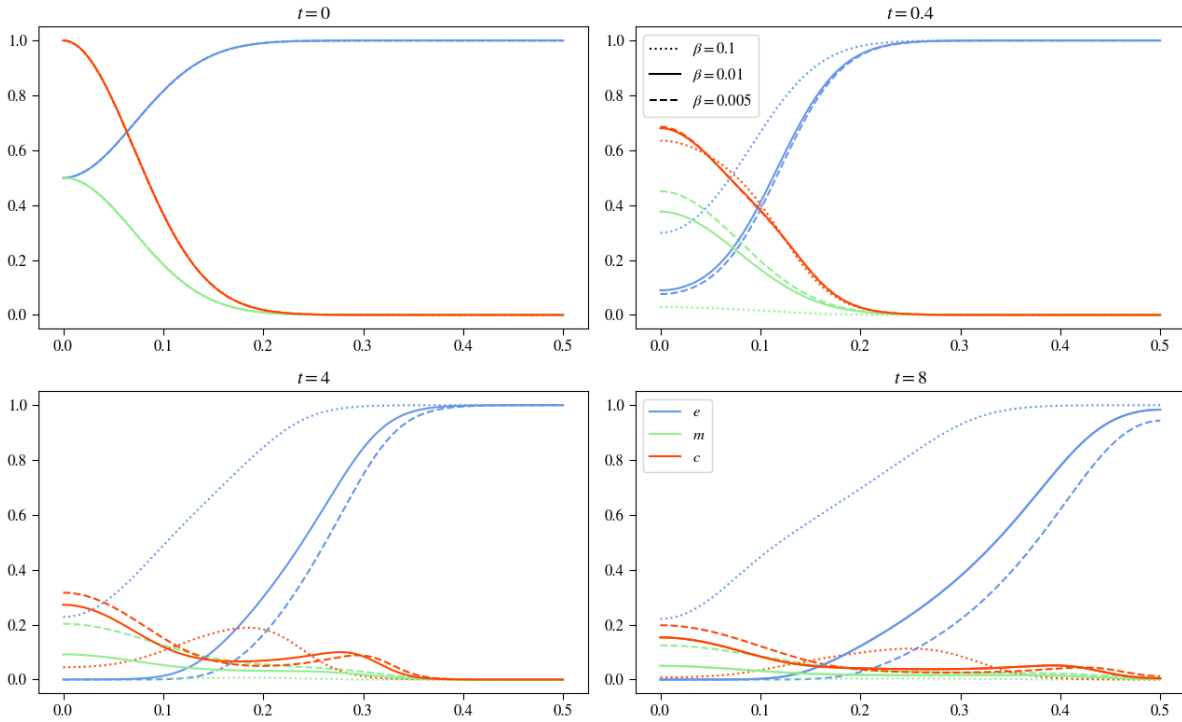


FIGURE 16. Plots show results for varying β while keeping the other parameters constant; in the images, you can see the effects of $\beta = 0.005$ in the dashed curve, $\beta = 0.1$ in the dotted curve and $\beta = 0.01$ in the solid line.

As we see from the results in figure 16, a value of $\beta = 0.1$ is sufficient to after already $t = 4$ reduce the MDE concentration to nearly zero. In our case, this decay rate proves too high, outpacing production entirely, with matrix-degrading enzyme concentration vanishing spacially and temporarily completely. The immediate decay of the MDEs causes a drastically slower ECM degradation, yet it has not stopped entirely since the tumor cells still produce matrix-degrading enzymes. This slow degradation of the extracellular matrix, as we saw previously, creates a haptotatic pull that lasts a lot longer in regions around the origin, which pulls, in this case, all of the cells outward to invade the tissue, leaving no primary lump of tumor cells at the origin. Since more MDEs are produced in regions with high tumor cell density, this also causes a more even degradation of the extracellular matrix, causing a more substantial stretch of the tumor cells.

In the other experiments, we can observe that with decreasing β and slowing down the decay of the matrix-degrading enzymes, first, the ECM degradation accelerates, and this

causes the effects of haptotaxis and diffusion to develop the two lumps of tumor cells, one staying at the center the other invading the tissue as we saw in all previous experiments.

Since the extracellular matrix can comprise many different organic and inorganic compounds, the degrading enzymes are also very diverse. This diversity results in different decay rates, so choosing the right one for a specific experiment can be crucial. While this variation describes the effects of different enzymes, it can also describe, like for the production of the MDEs, the influence of a drug to accelerate the decay of the matrix-degrading enzymes.

Cross-Variation

Having varied every model parameter, we saw accelerating effects on the invasion and countering effects. Now, it will be interesting to see how either supporting factors interplay and how countering factors affect the simulations, for example, how to increase both α and β if some balance can be found. Another exciting experiment will be on how diffusion and haptotaxis behave when increasing or decreasing both factors controlling them.

$d_c - \gamma$ Variation

We therefore started with varying d_c and γ , and studied for simplicity and overview reasons only the values on their distribution's borders interplaying.

Having set $d_c = 0.00005$ and $\gamma = 0.001$ we see no secession of the tumor cells, the effects of haptotaxis are too small leaving the tumor cells only subject to diffusion which results in an even distribution process over time, which also causes a slower invasion pace. Because the tumor cells stay in a lump with its maxima at the origin $x = 0$ the MDEs also take on their maximum there, moving farther out they also distribute very evenly. This staying with values around the origin of the MDEs causes a slower ECM degradation. Increasing $\gamma = 0.01$ we see that the effects of haptotaxis are now pregnantly visible with a very sharp maxima seen at $t = 4$, which equals the maxima of the remaining tumor cell lump at $x = 0$. Stronger influence of haptotaxis leads to a faster invasion pace of the tumor cells into the tissue and allowing to create matrix-degrading enzymes in their wake, causing a more even distribution compared to $\gamma = 0.001$ and also a faster ECM degrading process. Looking at the right side of the plot 17 we see the results for $d_c = 0.1$ here for both γ values diffusion overshadows the effects of haptotaxis completely, with after already $t = 0.4$ having a constant distribution of tumor cells throughout space. Due to this fast spread of tumor cells, the MDEs are also produced evenly throughout space, and an even faster ECM degradation.

$d_m - \eta$ Variation

Looking at low values for both d_m and η in the figure 18, the dotted curve in the left column, we see that slow diffusion of the matrix-degrading enzymes and slow degradation of the extracellular matrix causes the tumor cells to only develop one lump that invades space, due to stronger haptotactic exposition to a slower degraded ECM, to create larger values for $\nabla(c\nabla e)$, this is also observable for the higher diffusion values and lower ECM

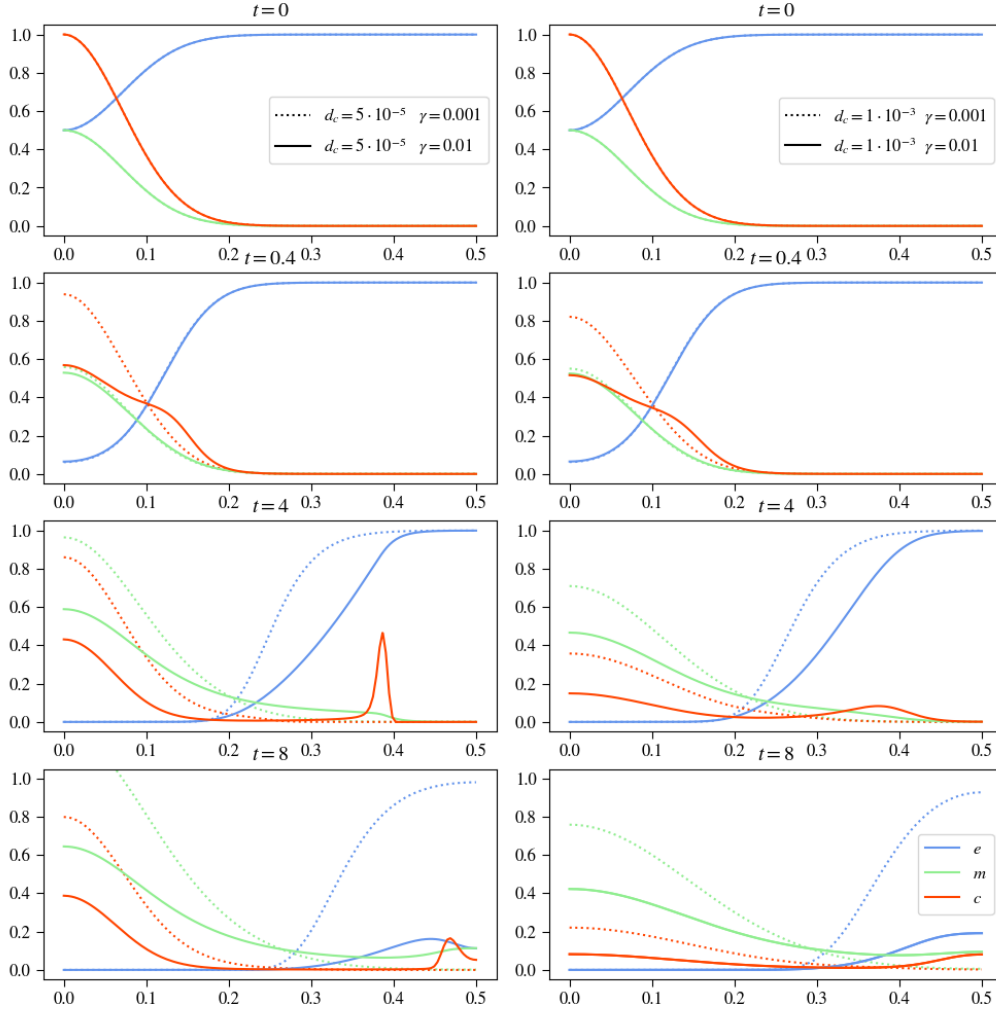


FIGURE 17. Plots show results for varying both d_c and γ whilst keeping the other parameters constant, in the images on the left d_c is set to $d_c = 0.00005$ with the solid line showing $\gamma = 0.01$ and the dotted line $\gamma = 0.001$ on the right d_c is set to $d_c = 0.1$ with the solid line showing $\gamma = 0.01$ and the dotted line $\gamma = 0.001$.

degrading factors. Having this single lump with a lower maxima and larger length causes the MDEs to produce more evenly farther away from the origin. The low value for the ECM degrading factor results in an overall slower ECM degradation. Looking on the solid line on the left column we see that increasing η enables the tumor cells to develop two hills, one staying at $x = 0$ and one invading space by haptotactic pull. Due to a higher density of tumor cells at the origin the MDEs produced there exceed a value of one and ECM degrading happens faster due to first the higher coefficient but also because of a faster invasion pace of matrix-degrading enzymes, due to faster invasion of the tumor cells. Increasing d_m to $d_m = 0.1$ causes the MDE concentration to flatten throughout space, taking on a constant distribution in space for one point in time, neglecting the values for η . Though η still has an influence on both tumor cell density and ECM concentration. We see that, as previously mentioned, for $\eta = 2$ the degrading happens so slow that the

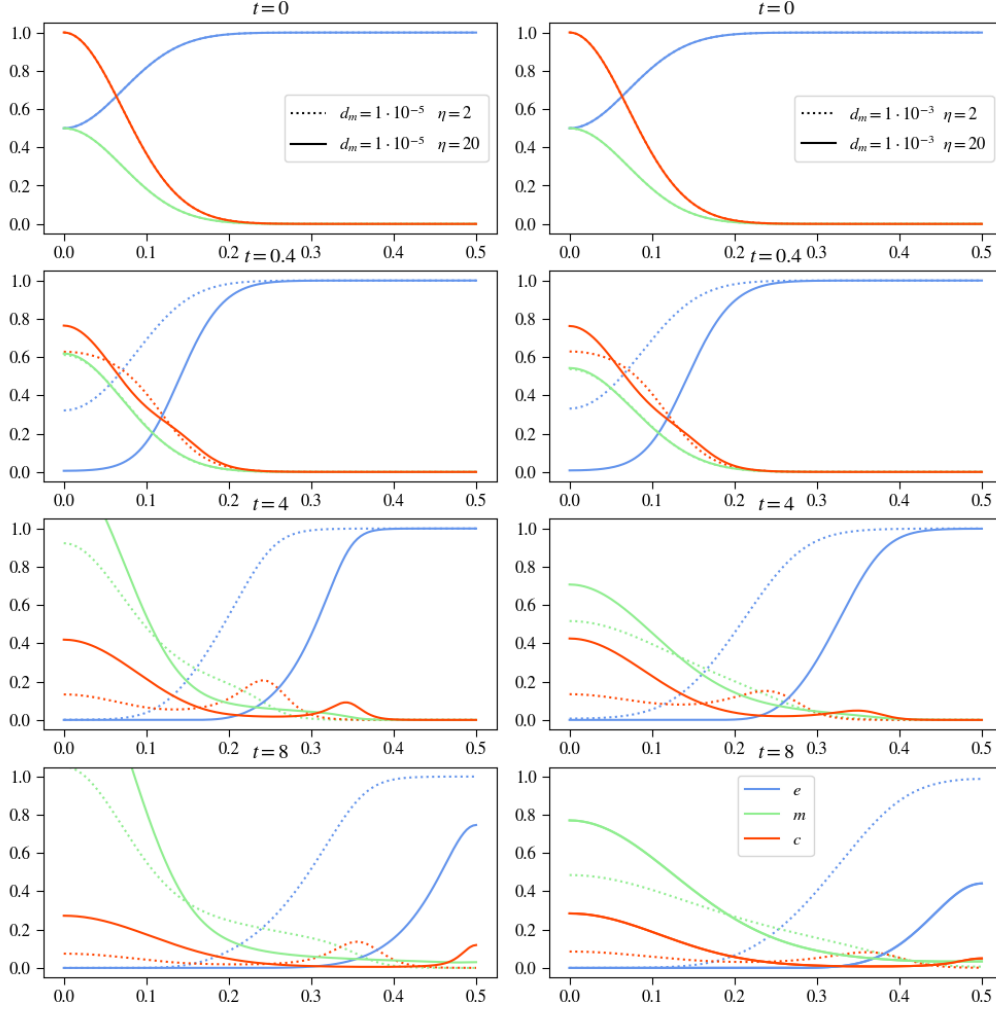


FIGURE 18. Plots show results for varying both d_m and η whilst keeping the other parameters constant, in the images on the left d_m is set to $d_m = 0.0000000001$ with the solid line showing $\eta = 2$ and the dotted line $\eta = 20$ on the right d_m is set to $d_m = 0.1$ with the solid line showing $\eta = 2$ and the dotted line $\eta = 20$.

tumor cells form only one lump invading the tissue, with its maxima travelling along the x-axis. In contrast to this for $\eta = 20$, we also see only one lump develop though this one stays with its maxima at the origin. For $\eta = 20$ we see that after $t = 4$ the ECM has almost completely degraded, making the formation of a secondary lump invading the tissue not possible due to too low haptotactic pull.

$\alpha - \beta$ Variation

Looking at figure 19 we see experimental results varying both α and β . For low MDE production but also low MDE decay we can see that the curve for the MDEs is still visible at up to $t = 4$, at $t = 8$ it is zero. We see that first the ECM degrading happens faster than for high β values and therefore the tumor cells develop two lumps with one invading the tissue the other staying at $x = 0$. The maxima for both lumps is lower than

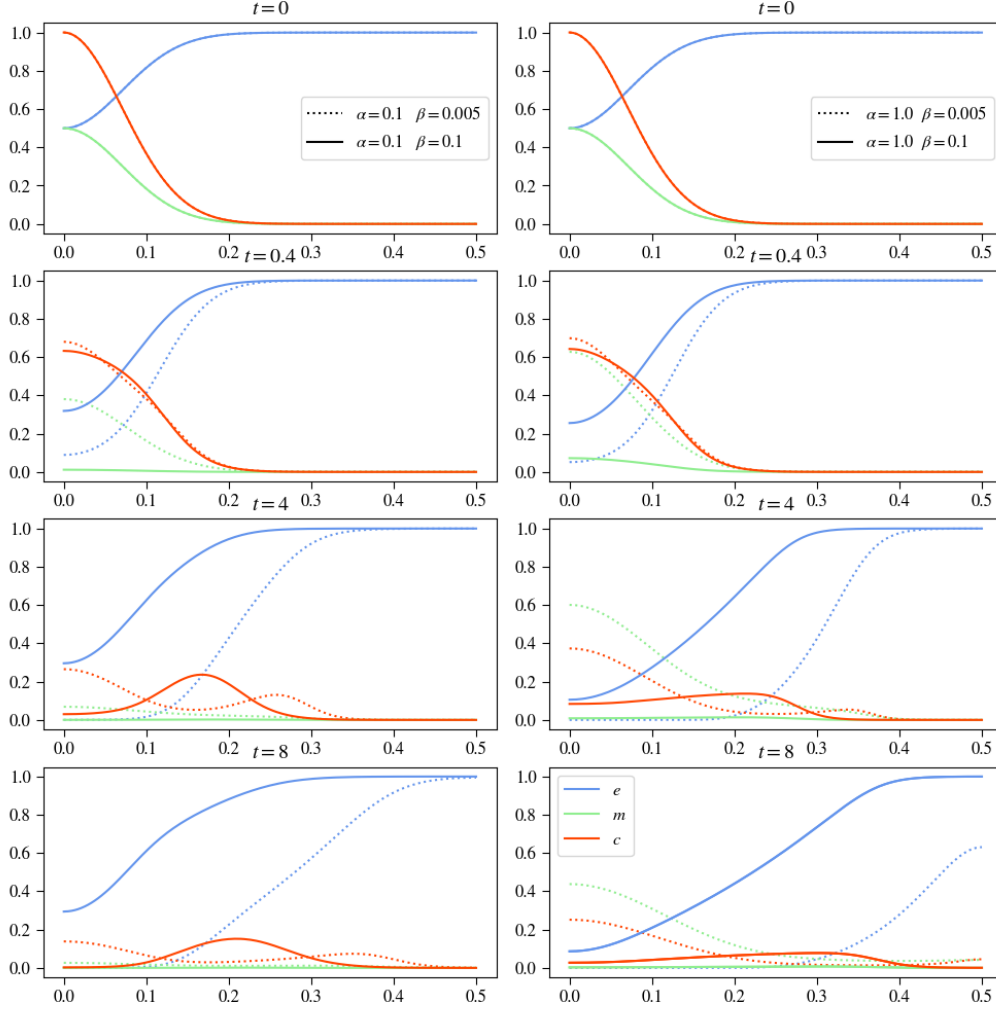


FIGURE 19. Plots show results for varying both α and β whilst keeping the other parameters constant, in the images on the left $\alpha = 0.1$ with the solid line showing $\beta = 0.005$ and the dotted line $\beta = 0.1$ on the right $\alpha = 1.0$ with the solid line showing $\beta = 0.005$ and the dotted line $\beta = 0.1$.

in previous experiments, though the cells seem to be more evenly distributed in between the two lumps. Increasing $\beta = 0.1$ the MDE curve seems to be zero after already $t =$ and stays there until the end of this experiment. This low concentration of MDEs casuses a slower ECM degrading process and therefore leads the tumor cells to only develop one lump, invading the space, with its maxima moving at the center of this lump. For $\alpha = 0.1$ both values for β have proven to be to high, decaying the matrix-degrading enzymes too fast to keep up with production. On the other hand increasing α to 1.0 and keeping $\beta = 0.05$, we see that production outweighs decay, with at the end of the experiment the MDEs still have a concentration of about 0.4 at $x = 0$. For this experiment we see that the tumor cells develop two lumps indicating that diffusion and haptotaxis effects are also in some balance, and ECM degradation seems to resemble due to similiarities with the basecase for the MDE curve, also the ECM degradation of the basecase experiment.

Increasing both α and β we see in the solid line of the right column of figure 19 that decay outweighs production again, after $t = 0.4$ we can only see a small remaining portion of matrix-degrading enzymes at the origin. This causes a slower ECM degradation and therefore to forming only one lump of tumor cells, due to too strong effects of haptotaxis, though this singular lump is stretched flat along the x-axis.

$d_m - \alpha - \beta$ Variation

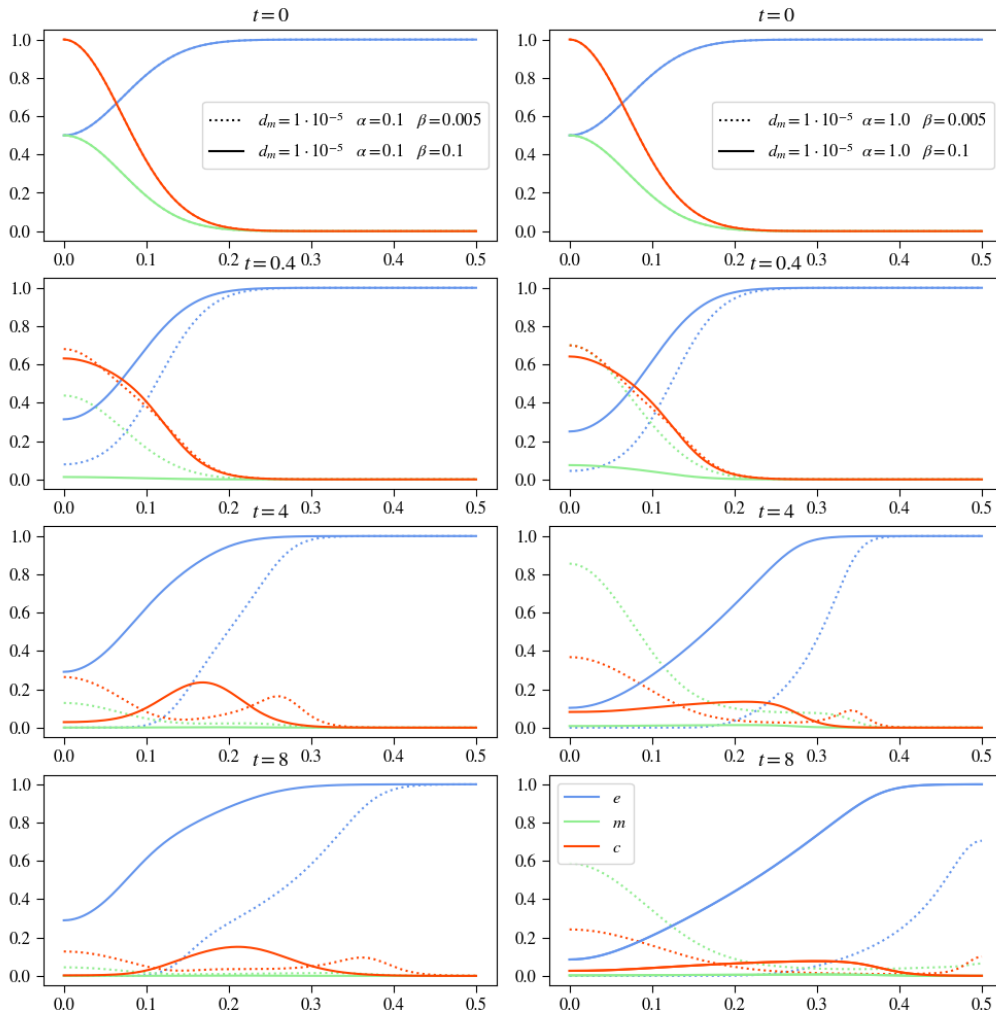


FIGURE 20. Plots show results for varying both α and β whilst keeping the other parameters constant, in the images on the left $\alpha = 0.1$ with the solid line showing $\beta = 0.005$ and the dotted line $\beta = 0.1$ on the right $\alpha = 1.0$ with the solid line showing $\beta = 0.005$ and the dotted line $\beta = 0.1$.

Experimenting with all parameters regarding the equation for the matrix-degrading enzymes required to split the results into two figures, 20 and 21, due to clarity reasons. We are first going to take a look at the results in figure 20, to see the effect of a decreased diffusion coefficient for the MDEs. We observe that with having $\alpha = 0.1$ and $\beta = 0.005$ the ECM degradation happens faster due to having a higher MDE concentration, because

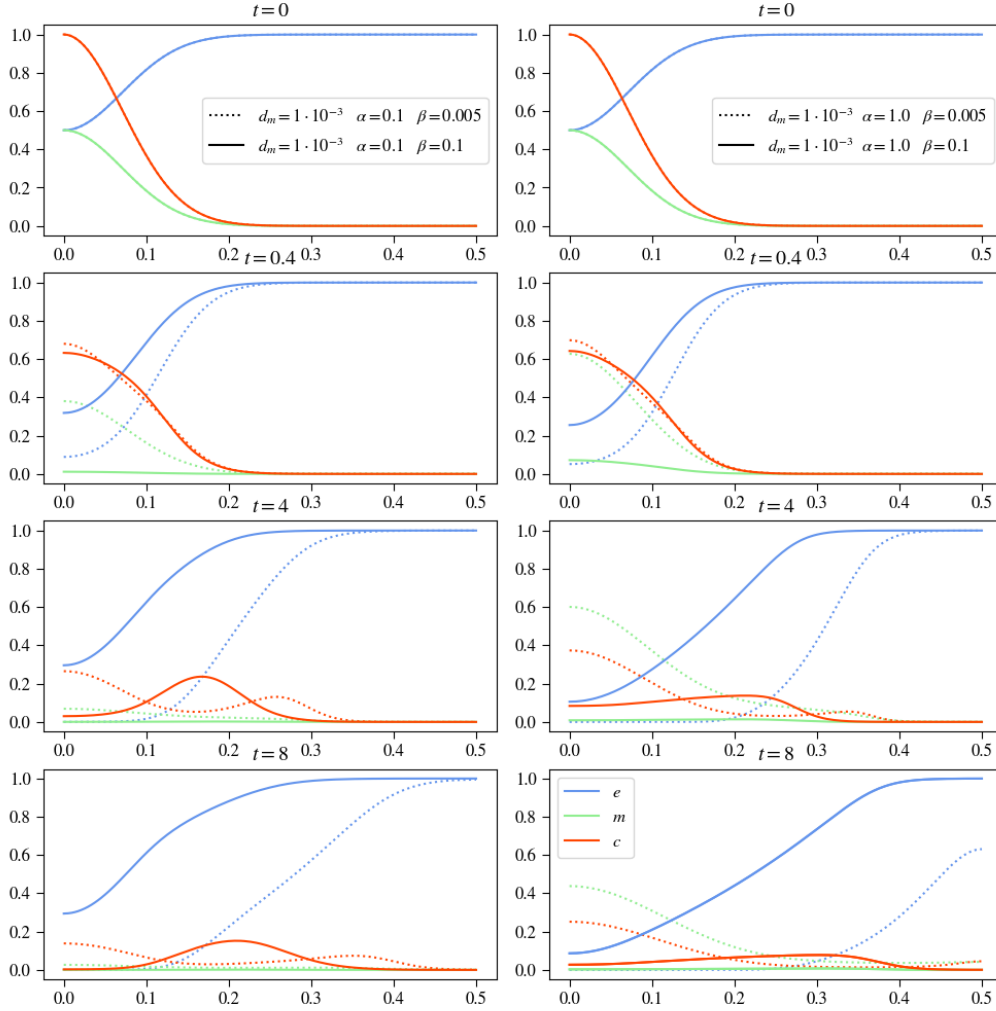


FIGURE 21. Plots show results for varying both α and β whilst keeping the other parameters constant, in the images on the left $\alpha = 0.1$ with the solid line showing $\beta = 0.005$ and the dotted line $\beta = 0.1$ on the right $\alpha = 1.0$ with the solid line showing $\beta = 0.005$ and the dotted line $\beta = 0.1$.

of lower MDE decay. Which also increases the separation of the effects of haptotaxis and diffusion on the tumor cells, separating them into two lumps, one being pulled them along the ECM faster into the tissue the other staying at the origin. Though the MDE concentration diminishes over time we can still see little remaining concentration at the end at $t = 8$. Increasing β diminishes the MDE concentration sharply, slowing down the ECM degrading process, which increases the effect of haptotaxis over diffusion to pull all of the tumor cells away from the origin to invade the tissue as one lump though at a slower pace. Over time we can see that as expected the tumor cell density's maximum is located approximately right below where $\nabla(c\nabla e)$ is highest.

Looking at the experiments with higher α values we can see that for lower β values the MDE concentration oscillates up and down over time, which indicates that with this configuration of α and β values we found a balancing point. For higher β values we

cannot observe this balance, since in this case the MDEs have nearly decayed after $t = 4$. Having such differences in the MDE concentration we can also see big differences in the ECM concentration. Here we see that as expected with $\beta = 0.005$ the ECM degradation happens a lot faster than having $\beta = 0.1$. These changes in the ECM concentration also affect the tumor cell density. Like in the experiments with $\alpha = 0.1$ the results for having higher β lead to only one lump invading the tissue with a more even distributed density along the x-axis, whereas lower β values made the diffusion and haptotaxis differentiable forming two lumps one to stay at the origin, one to invade the tissue outwards.

Next we are investigating how changing d_m as well will affect the system, looking at figure 21. First of all it is to say that as with varying d_m only the diffusion here is also strong enough to in most cases completely evenly distribute the matrix-degrading enzymes in all of the space after already the fourth step in time.

On the left side we see the experiments with low α values and see that less decay of the MDEs leads to slower ECM degradation. Due to the very even distribution of the MDEs we see for both cases a more evenly degradation of the ECM, with overall lower gradients. This results in a longer exposition of haptotatic effects on the tumor cells to form only lump invading the tissue with a moving maximum, though for a lower β factor we see that a larger is staying at the origin since the haptotatic pull here is weaker due to having also a more evenly distributed tumor cell density.

Looking at the right side of figure 21 we see with increased α the results regarding the tumor cell density differ strongly. Whereas on the left side we saw that there was always one lump to invade the cells with its maximum moving below where $\nabla(c\nabla e)$ is strongest, we see that for low β the lump of tumor cell stays with its core at the origin at $x = 0$, where also its maximum is, and invades the tissue with no leading edge. This shows the effect of a both sufficiently fast and efficient degradation of extracellular matrix. Here we see diffusion as the main factor for the movement of the tumor cells since the haptotatic pull is very low, due to small gradients of e only. For the other curves we can observe that as before with rising β the ECM degradation pace slows down, in the last point in time the difference β causes is pregnantly visible with for low β the ECM has been degraded completely but for high β there is still a considerable concentration. Looking at the MDE concentration we can also see clear differences regarding the influence of the diffusion on the MDE decay. Though the MDE concentration with high diffusion is more evenly distributed, its overall volume in space is clearly lower than for low diffusion terms, with same α and β configurations.

4.2 2D Results with Proliferation and Renewal - Homogenous ECM

In this section we are going to inspect how introducing tumor cell proliferation and extracellular matrix renewal influences the system. Modelled as logistical growth terms, with a limiting factor of spacial occupation, the parameters μ_1 for tumor cell proliferation and μ_2 for extracellular matrix renewal describe their influences. In the previous experiments those parameters were also incorporated, though set to zero. Instead of treating them as parameters to vary, we are inspecting the whole system a new, since they have the

potential to drastically change the resulting simulations.

Tumor cell proliferation describes the natural ability of cells to proliferate. Though in the case of the tumor cells the production signalling comes from themselves, surpassing the control chain that limits normal cells to proliferate uncontrollably.

The extracellular matrix is a naturally dynamic structure that undergoes continuous degradation and remodelling. It does this in order to secure tissue development, wound repair tasks, regulate cellular functions or many more tasks. In a model describing the ECM it is crucial to introduce a factor that incorporates these remodelling processes.

As in section 4.1, we are using the same initial conditions for all three variables under the assumption we have a homogenous ECM structure. Figure 3 depicts these initial conditions on the three variables c, e, m at dimensionless time $t = 0$.

Figure	Linestyle	d_c	γ	μ_1	η	μ_2	d_m	α	β
22	$5 \cdot 10^{-4}$	0.0055	0	10	0	$1 \cdot 10^{-3}$	0.3564	0
22	———	$5 \cdot 10^{-4}$	0.0055	0.1	10	0.5	$1 \cdot 10^{-3}$	0.3564	0
23	$1 \cdot 10^{-3}$	0.0055	0.1	10	0.5	$1 \cdot 10^{-3}$	0.3564	0
23	———	$1 \cdot 10^{-4}$	0.0055	0.1	10	0.5	$1 \cdot 10^{-3}$	0.3564	0
23	- - - -	$5 \cdot 10^{-5}$	0.0055	0.1	10	0.5	$1 \cdot 10^{-3}$	0.3564	0
24	$5 \cdot 10^{-4}$	0.002	0.1	10	0.5	$1 \cdot 10^{-3}$	0.3564	0
24	———	$5 \cdot 10^{-4}$	0.008	0.1	10	0.5	$1 \cdot 10^{-3}$	0.3564	0
24	- - - -	$5 \cdot 10^{-4}$	0.01	0.1	10	0.5	$1 \cdot 10^{-3}$	0.3564	0
25	$5 \cdot 10^{-4}$	0.0055	0	10	0.5	$1 \cdot 10^{-3}$	0.3564	0
25	———	$5 \cdot 10^{-4}$	0.0055	0.5	10	0.5	$1 \cdot 10^{-3}$	0.3564	0
25	- - - -	$5 \cdot 10^{-4}$	0.0055	1.0	10	0.5	$1 \cdot 10^{-3}$	0.3564	0
26	$5 \cdot 10^{-4}$	0.0055	0.1	2	0.5	$1 \cdot 10^{-3}$	0.3564	0
26	———	$5 \cdot 10^{-4}$	0.0055	0.1	12	0.5	$1 \cdot 10^{-3}$	0.3564	0
26	- - - -	$5 \cdot 10^{-4}$	0.0055	0.1	20	0.5	$1 \cdot 10^{-3}$	0.3564	0
27	$5 \cdot 10^{-4}$	0.0055	0.1	10	0.1	$1 \cdot 10^{-3}$	0.3564	0
27	———	$5 \cdot 10^{-4}$	0.0055	0.1	10	0.6	$1 \cdot 10^{-3}$	0.3564	0
27	- - - -	$5 \cdot 10^{-4}$	0.0055	0.1	10	1.0	$1 \cdot 10^{-3}$	0.3564	0
28	$5 \cdot 10^{-4}$	0.0055	0.1	10	0.5	$1 \cdot 10^{-3}$	0.3564	0
28	———	$5 \cdot 10^{-4}$	0.0055	0.1	10	0.5	$1 \cdot 10^{-4}$	0.3564	0
28	- - - -	$5 \cdot 10^{-4}$	0.0055	0.1	10	0.5	$1 \cdot 10^{-5}$	0.3564	0
29	$5 \cdot 10^{-4}$	0.0055	0.1	10	0.5	$1 \cdot 10^{-3}$	0	0
29	———	$5 \cdot 10^{-4}$	0.0055	0.1	10	0.5	$1 \cdot 10^{-3}$	0.6	0
29	- - - -	$5 \cdot 10^{-4}$	0.0055	0.1	10	0.5	$1 \cdot 10^{-3}$	1.0	0
30	$5 \cdot 10^{-4}$	0.0055	0.1	10	0.5	$1 \cdot 10^{-3}$	0.3564	0.1
30	———	$5 \cdot 10^{-4}$	0.0055	0.1	10	0.5	$1 \cdot 10^{-3}$	0.3564	0.01
30	- - - -	$5 \cdot 10^{-4}$	0.0055	0.1	10	0.5	$1 \cdot 10^{-3}$	0.3564	0.005
31 - left	$5 \cdot 10^{-4}$	0.0055	0.1	10	0.1	$1 \cdot 10^{-3}$	0.3564	0
31 - left	———	$5 \cdot 10^{-4}$	0.0055	0.1	10	1.0	$1 \cdot 10^{-3}$	0.3564	0
31 - right	$5 \cdot 10^{-4}$	0.0055	1.0	10	0.1	$1 \cdot 10^{-3}$	0.3564	0

continued on next page

Figure	Linestyle	d_c	γ	μ_1	η	μ_2	d_m	α	β
31 - right	——	$5 \cdot 10^{-4}$	0.0055	1.0	10	1.0	$1 \cdot 10^{-3}$	0.3564	0
32 - left	$1 \cdot 10^{-5}$	0.001	0.1	10	0.5	$1 \cdot 10^{-3}$	0.3564	0
32 - left	——	$1 \cdot 10^{-5}$	0.001	1.0	10	0.5	$1 \cdot 10^{-3}$	0.3564	0
32 - right	$1 \cdot 10^{-5}$	0.01	0.1	10	0.5	$1 \cdot 10^{-3}$	0.3564	0
32 - right	——	$1 \cdot 10^{-5}$	0.01	1.0	10	0.5	$1 \cdot 10^{-3}$	0.3564	0
33 - left	$1 \cdot 10^{-3}$	0.001	0.1	10	0.5	$1 \cdot 10^{-3}$	0.3564	0
33 - left	——	$1 \cdot 10^{-3}$	0.001	1.0	10	0.5	$1 \cdot 10^{-3}$	0.3564	0
33 - right	$1 \cdot 10^{-3}$	0.01	0.1	10	0.5	$1 \cdot 10^{-3}$	0.3564	0
33 - right	——	$1 \cdot 10^{-3}$	0.01	1.0	10	0.5	$1 \cdot 10^{-3}$	0.3564	0
34 - left	$5 \cdot 10^{-4}$	0.0055	0.1	2	0.1	$1 \cdot 10^{-3}$	0.3564	0
34 - left	——	$5 \cdot 10^{-4}$	0.0055	0.1	2	1.0	$1 \cdot 10^{-3}$	0.3564	0
34 - right	$5 \cdot 10^{-4}$	0.0055	0.1	20	0.1	$1 \cdot 10^{-3}$	0.3564	0
34 - right	——	$5 \cdot 10^{-4}$	0.0055	0.1	20	1.0	$1 \cdot 10^{-3}$	0.3564	0

TABLE 2. Overview of all experiments conducted for the model with proliferation and renewal producing 2D output

As in section 4.1 we see in table 2 a detailed overview of all the experiments done in this section and the parameters used to produce the results. As before do most figures describe multiple experiments, the linestyle of the curve in the figure determines which experiment exactly is described by the set of parameters.

4.2.1 Basecase Analysis

It makes sense to establish a basecase to compare the following parameter analysis results against it. In figure 22 you can see how introducing tumor cell proliferation and extracellular matrix renewal changes the outcome of the simulation. For this we used the values $\mu_1 = 0.1$ and $\mu_2 = 0.5$ according to the only experiment found for this system of equations in the paper of Kolev et al. [12].

Comparing this new basecase to our initial model's basecase we can see the influences of both μ_1 and μ_2 , as for the tumor cell density curve is visibly higher than without proliferation, causing a higher production of matrix-degrading enzymes, which would lead to faster ECM degradation, though this is countered by the renewal factor μ_2 causing the ECM concentration to be higher at the end, at $t = 8$, than in the initial basecase experiment.

4.2.2 Parameter Analysis

For the Parameter Analysis of the model with proliferation and renewal we are focusing on comparing the results of the updated model with the results produced by the model without renewal and proliferation, this will point out again the influence of μ_1 and μ_2 on the system.

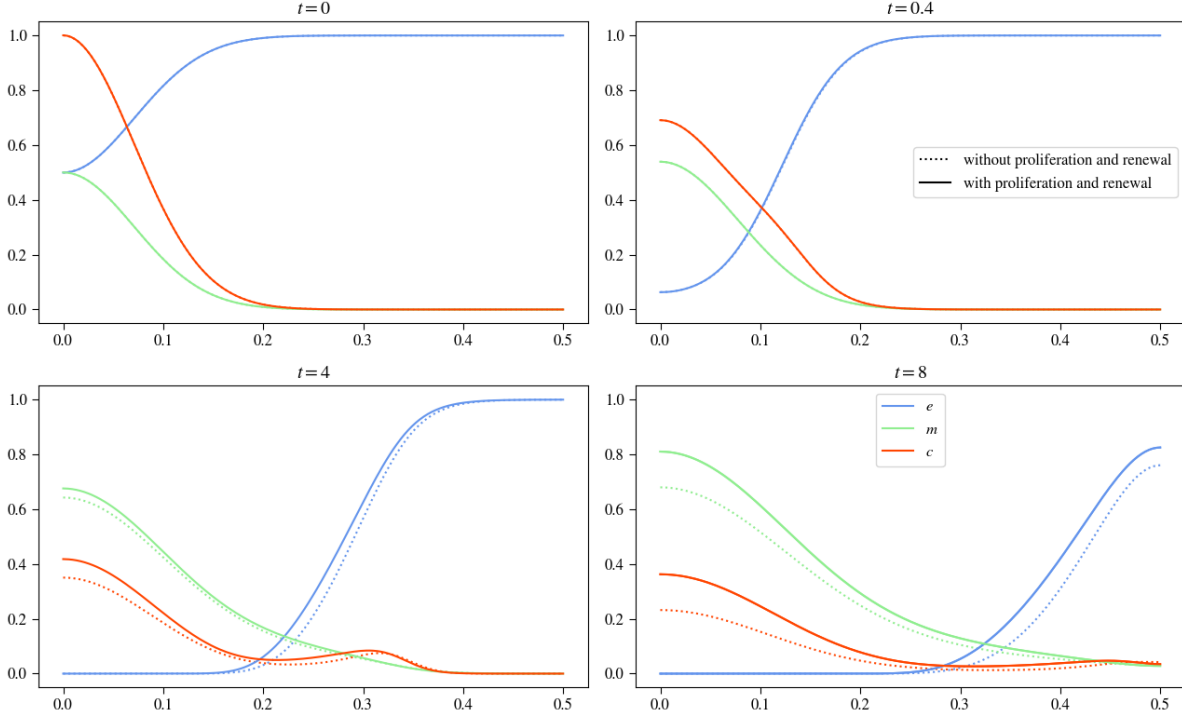


FIGURE 22. Describing the updated basecase, in the image above only the updated basecase is plotted, below it is compared to the initial basecase.

d_c Variation

Varying d_c with proliferation terms, we see the same effects as without proliferation. Higher values for d_c cause a stronger influence of diffusion and a weaker for the haptotaxis, which leads to a curve with less or none of a leading edge invading the space, but to a faster rather constant distribution throughout space. The MDE concentration follows this behaviour, depending on its production on the tumor cell density distribution in space and the ECM is decayed faster, the faster the tissue is invaded, thus the higher the diffusion factor is. Comparing them we see little differences, only tumor cell density and ECM are raised a little in each plot due to the renewal and proliferation factors, which in turn also causes a higher MDE concentration, due to higher tumor cell densities.

γ Variation

When we look at γ we also can see the same effects as the model without proliferation shows, with the adjustments as varying d_c , with raised curves for all variables. Increasing γ means increasing haptotaxis effects, pulling the tumor cells stronger towards the extracellular matrix molecules, which causes a faster invasion pace and also a higher density of tumor cells invading the tissue, but a lower staying at the center at $x = 0$. This also means that the ECM degrading process happens faster and the MDEs are more evenly distributed through space the higher γ is. As mentioned above the same effects come in this experiment, introducing proliferation and renewal, with higher values for tumor

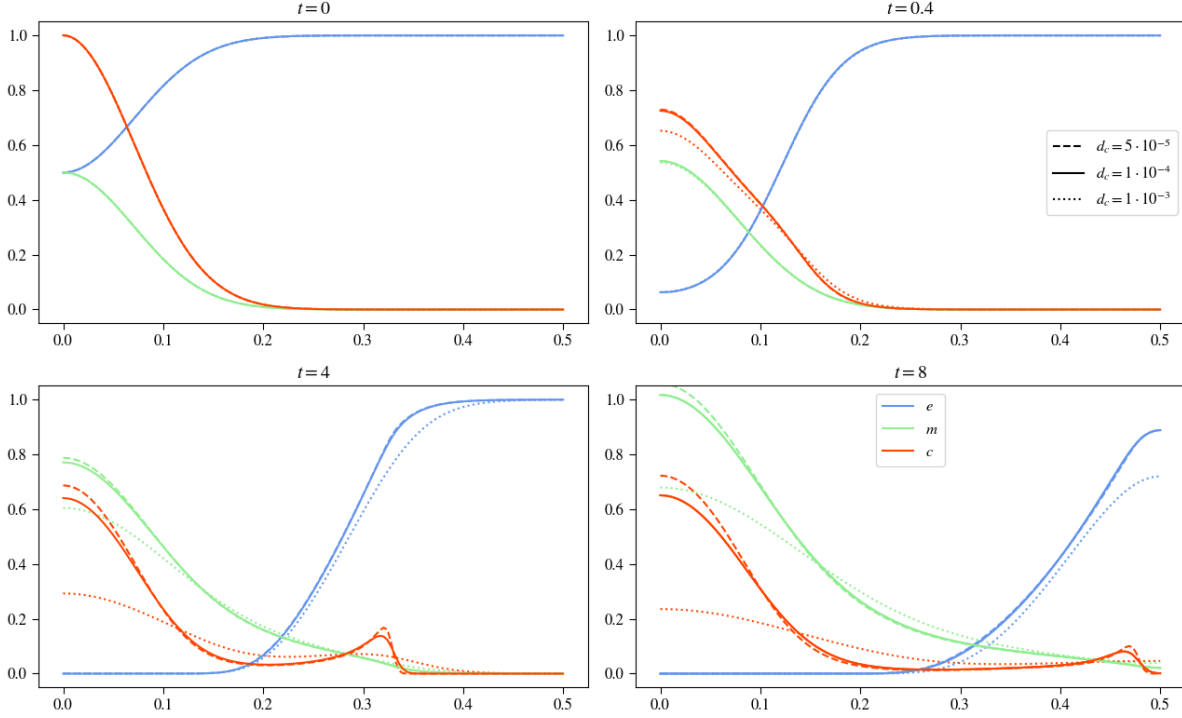


FIGURE 23. Plots show results for varying d_c whilst keeping the other parameters constant

cell density, MDE and ECM concentration especially at the later points in time clearly depictable. It is interesting to observe that though introducing a renewal factor for the extracellular matrix, the proliferation of the tumor cells causes a faster production of matrix-degrading enzymes, which makes the system produce nearly the same results as without proliferation and renewal concerning the ECM concentration, still it is to say that introducing the renewal of the ECM results in overall slightly higher concentrations of it.

μ_1 Variation

The parameter μ_1 describes the proliferation of the tumor cells, using Kolev et al's estimate in [12] we assume an even distribution with $\mu_1 \sim U[0.1, 1.0]$. Introducing this factor we can, with an increase of the total amount of tumor cells, expect a faster production of the matrix-degrading enzymes and also a faster degradation of the ECM. Though the effect of the faster ECM degradation might be damped by also introducing a renewal term for it, we can especially for higher μ_1 values expect to dominate the simulations and accelerate ECM degradation.

Since the basecase, using Kolev et al's values, sets the proliferation rate of the tumor cells to $\mu_1 = 0.1$ we consider in the dotted experiment the effects of only introducing the renewal of the ECM.

The effects of μ_1 take some time to act, as we can see no deviations for all the experiments in figure 25 at $t = 0.4$.

At the next point in time at $t = 4$, the differences are striking, concerning all variables.

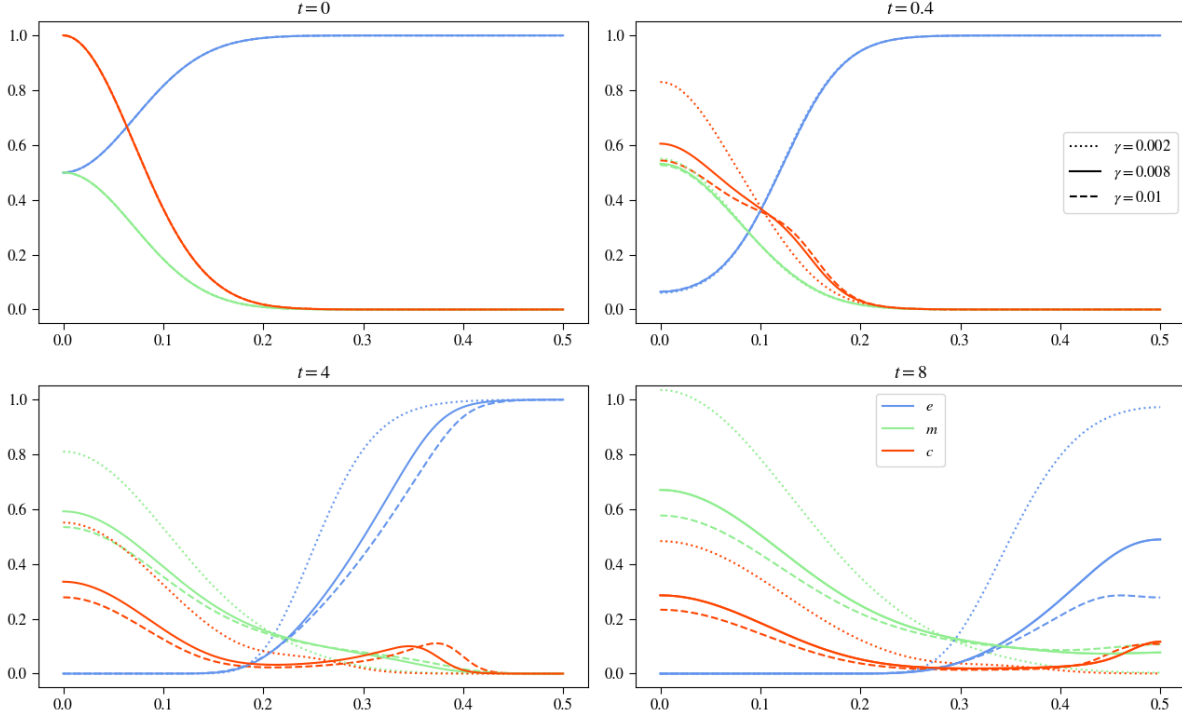


FIGURE 24. Plots show results for varying γ whilst keeping the other parameters constant.

With a higher proliferation factor of the tumor cells, the MDE concentration also rises clearly and the ECM degradation is also accelerated. Yet at this point in time the deviations regarding the curve for the ECM concentration are still subtle.

It looks different in the last point in time at $t = 8$. As mentioned above does an increase of total tumor cells drastically increase the MDE concentration and accelerates the ECM degradation.

Introducing μ_1 means introducing one of the hallmarks of cancer; sustaining proliferative signalling, which makes the tumor cells themselves responsible for producing them, instead of requiring other hormones or enzymes to trigger growth signalling. Setting $\mu_1 = 0$ could be the consequences of a drug working, hindering growth signalling.

η Variation

As we compare the η variation between with and without proliferation and renewal models we see mostly the same effects. For the solid and dashed curves we see little though the curves of the new model are all slightly raised. Looking at $\eta = 0$ we see some interesting deviations, at the time point $t = 0.4$ the plots still look rather similar, but looking at $t = 4$ we see that the curve of the tumor cells has a more even distribution along the x-axis and also its maximum is visibly lower with value of about 0.2 at $x = 1.4$ instead of 0.25 at $x = 1.3$. This behaviour is due to the renewal of the ECM, where without proliferation this curve stayed constant throughout the experiment, here it can increase, which it does altering the slope of the curve and therefore influencing the haptotactic pull for

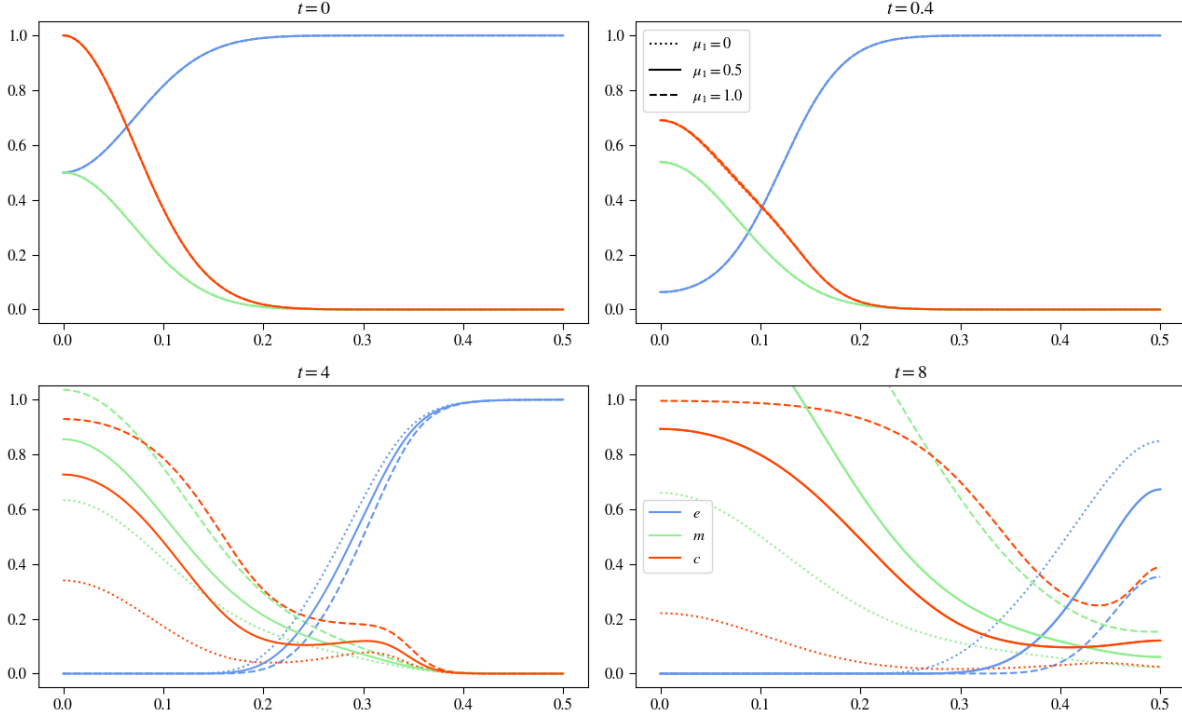


FIGURE 25. Plots show results for varying μ_1 whilst keeping the other parameters constant.

the tumor cells, additionally to this the other two experiments showed a visible increase of the tumor cell density and the matrix-degrading enzyme concentration, but only a slight for the ECM concentration, here we can see no increasing of area for the tumor cell density at all. The renewal of the ECM counters the proliferation of the tumor cells and the slowed ECM degrading process in such a way that at the last two point in time we see that the ECM has visibly increased, with both curves ECM and tumor cells almost mirroring each other. Summing up the areas of both variables we see that they together occupy the space completely needed for the logistical growth terms, which means that proliferation and renewal will play no more important role continuing with this experiment as they have reached a equilibrium state and cancel each other out.

μ_2 Variation

The parameter μ_2 describes the renewal processes of the extracellular matrix molecules. Also using Kolev et al's estimate in [12] we can assume an even distribution with $\mu_2 \sim U[0.1, 1.0]$. In natural processes the renewal of the extracellular matrix is important to regulate cell differentiation and wound repair for example [14]. This renewal process as we see in figure 27 takes some time to show effects. There are no deviations for the experiments after $t = 0.4$.

Looking at the results later at $t = 4$ the differences are still subtle. Increasing μ_2 slows down the extracellular matrix degradation process and with this affects the motility of the tumor cells, pulling less of them outwards into the surrounding tissue. The MDE

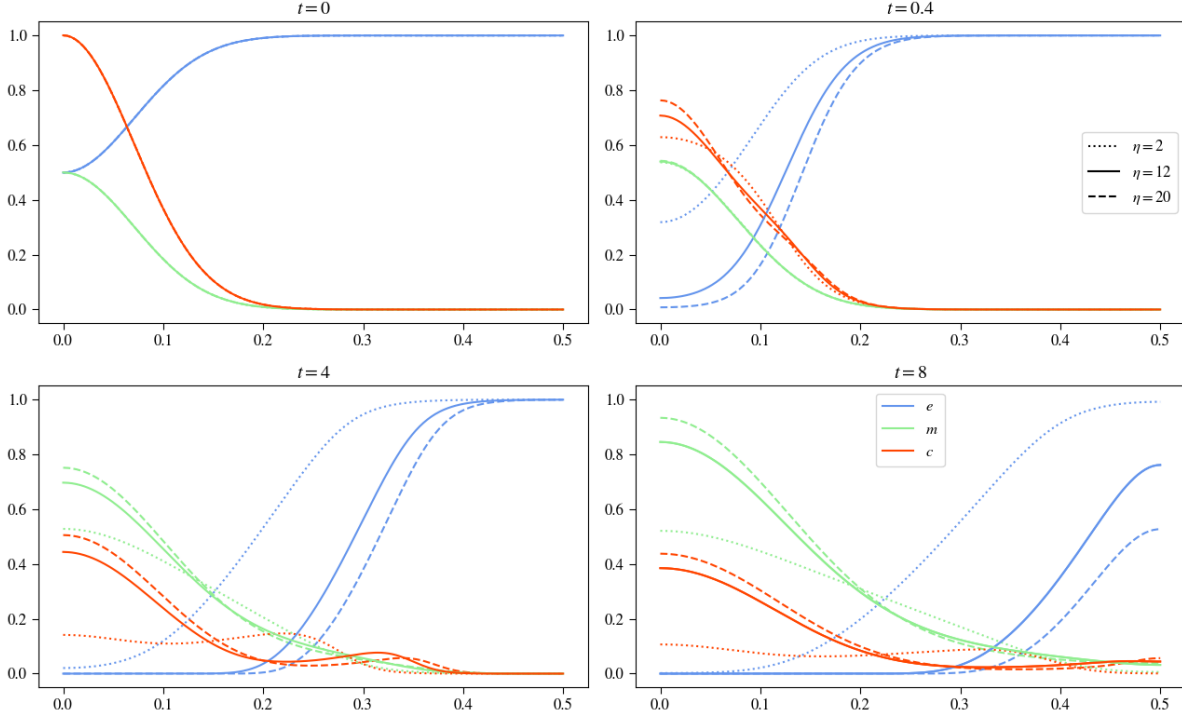


FIGURE 26. Plots show results for varying η whilst keeping the other parameters constant.

concentration nearly overlays completely, with a minimal higher concentration for the lowest μ_2 experiment at the origin, due to the also slightly higher tumor cell density at the origin.

The differences at the last point in time at $t = 8$ are still minor compared to varying the other parameters. As mentioned before does the slowed ECM degradation diminish haptotactic effects, which leads to slightly less matrix-degrading enzymes concentration at the origin.

We see that varying the ECM renewal rate at this magnitude shows little influence on the resulting simulations.

At this point it is important to say that the renewal rates for tissue in the human body strongly vary. Comparing for example bone tissue with connective tissue, we see these processes at highly different time scales. Out of lack of experimental data for this parameter we only investigated Kolev et al's estimates, but considering realistic cases, it is important to have better measures for this parameter.

d_m Variation

Comparing the results varying the diffusion factor of the matrix-degrading enzymes does as before yield only minor differences between the initial and updated model. As observed before the tumor cell density's curve and the MDE concentration's curves are slightly raised due to proliferation of the tumor cells. The ECM curve for two lower values of varying d_m though seem to be subject to little to no change, only for very high values of

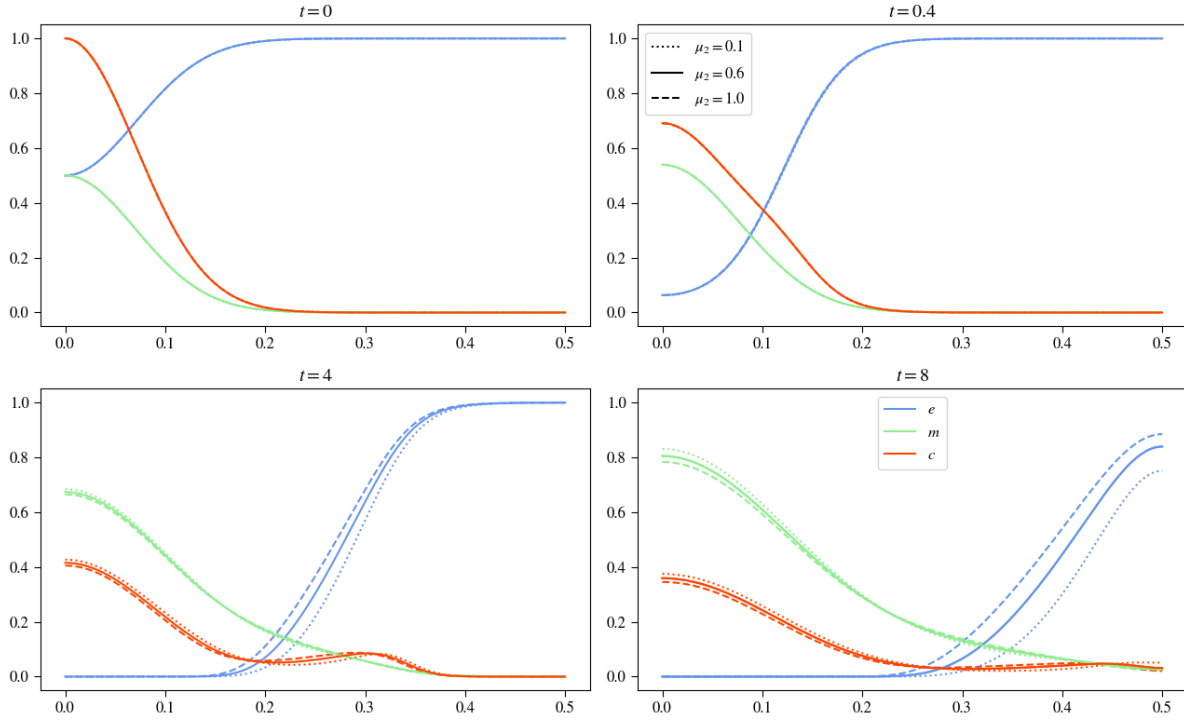


FIGURE 27. Plots show results for varying μ_2 whilst keeping the other parameters constant.

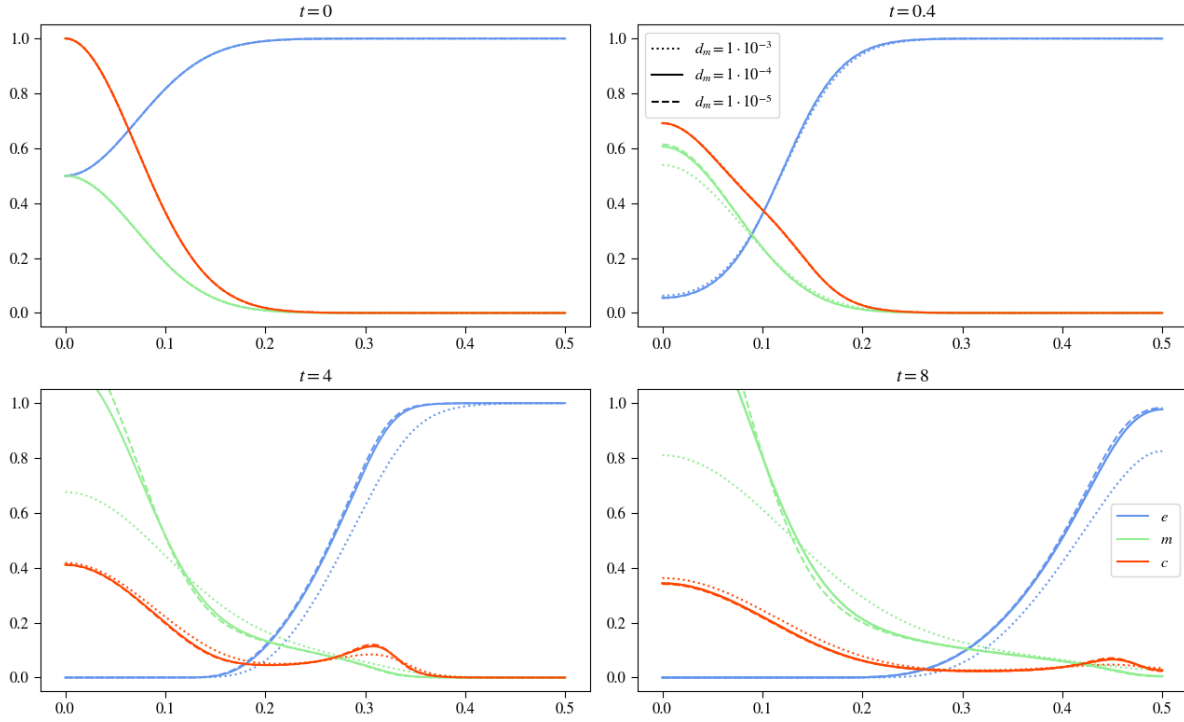


FIGURE 28. Plots show results for varying d_m whilst keeping the other parameters constant.

d_m we can see that it is clearly raised comparing it to the model without renewal. The other two curves take off at the some point along the x-axis and finish at the same values for their ECM concentration. Looking at the tumor cell density curves for those d_m values we see that towards $x = 0.5$ they don't describe a as steep bump as the initial model. This causes to have little less MDE concentration as well, which is responsible for the seemingly unchanged behaviour of the extracellular matrix concentration.

α Variation

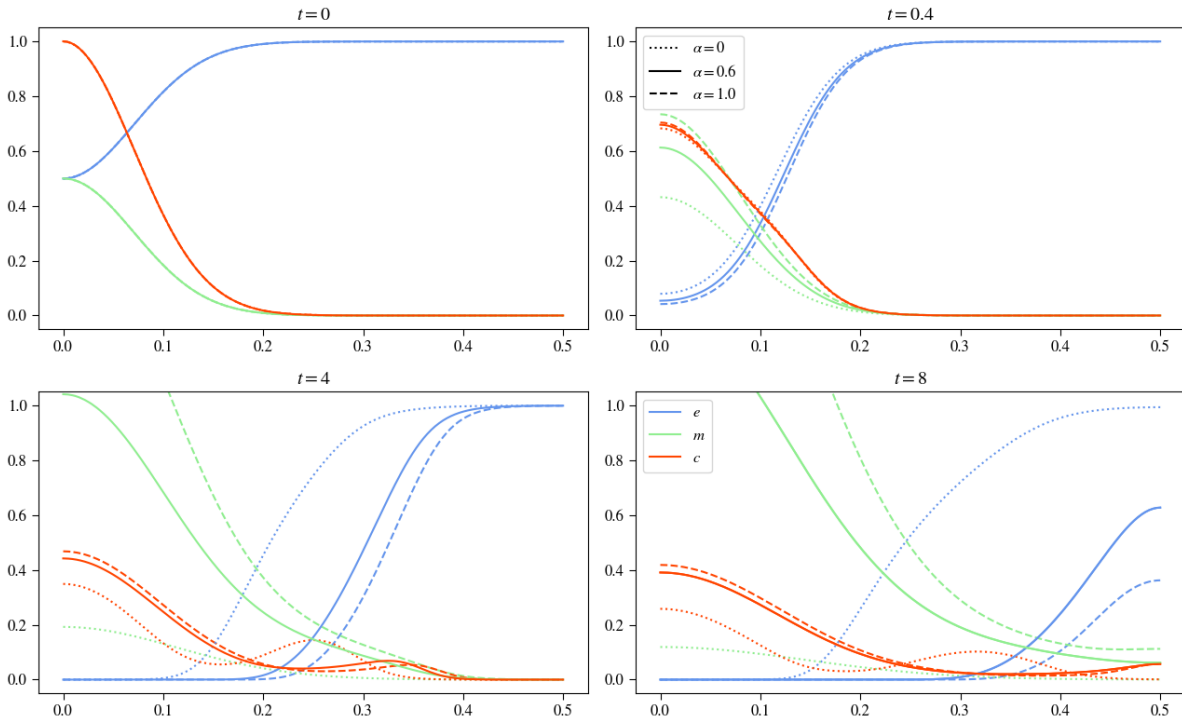


FIGURE 29. Plots show results for varying α whilst keeping the other parameters constant.

Taking a look at comparing the α -variation yields more interesting results since, μ_1 acts as a secondary MDE production effect by producing tumor cells which in turn produce the matrix-degrading enzymes. We see that though the overall shape and effects to be observed are the same, after $t = 4$ the model with proliferation exceeds one at the origin for the MDE concentration for the two higher α experiments, where in the model without proliferation only the one with the highest α value did. The tumor cell density curve is slightly raised, which allows the MDE concentration. Though the higher values for the MDEs leave the ECM degrading process untouched with not clearly visible difference between the initial model and the updated one.

β Variation

Considering β we can expect that with the introduction of μ_2 the ECM degradation will be slowed considerably with rising β , since this does not only reduce the MDE concentration

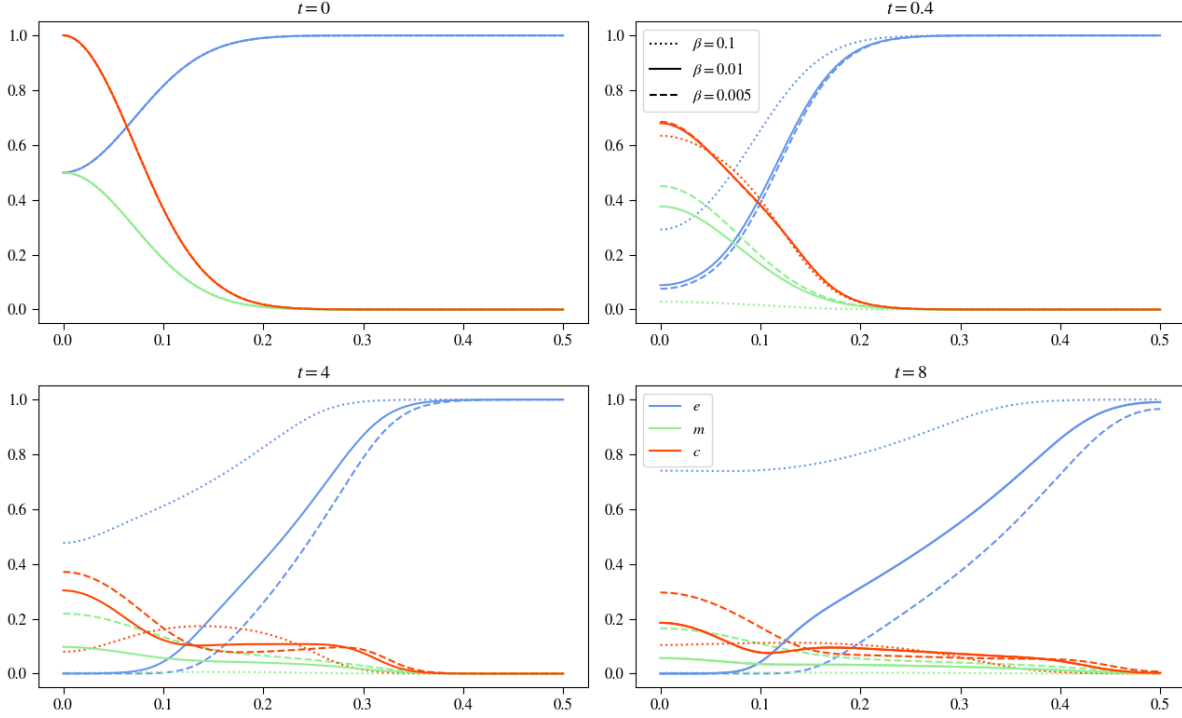


FIGURE 30. Plots show results for varying β whilst keeping the other parameters constant.

but does also renew the ECM. Looking at the plots we can see exactly this behaviour in the dotted line, which shows the experiment results for the highest β value of 0.1. Though even at the end it has an overall area that is slightly less than the initial condition we can see going from timestep $t = 0.4$ to $t = 4$ that MDE decay and ECM renewal were sufficiently strong to restore the ECM and going from $t = 4$ to $t = 8$ we see this behaviour again, renewing the ECM. The other two experiments for β showed no effects as strong as with $\beta = 0.1$, yet we can still see the effects of proliferation and renewal especially clear in the solid line, $\beta = 0.01$ at the last point in time, where we can observe a visible increase of both ECM and tumor cell density. In this experiment we see that β is a little too low to counter the effects of ECM degradation, going from $t = 4$ to $t = 8$ we see a clear decline of ECM concentration though it is not as striking as for $\beta = 0.005$.

Cross Variation

$\mu_1 - \mu_2$ Variation

The effects to observe in this cross variation take some time as did the separate variations of both μ_1 and μ_2 . for both $\mu_1 = \mu_2 = 0.1$ we see that slower ECM renewal and slower tumor cell proliferation increase the degrading process of the extracellular matrix and with this affect the haptotaxis effect to increase slightly. At the center a lump remains that has a maximum a little higher than for the experiment with $\mu_2 = 1.0$ and also the invasion of the tissue has proceeded a little faster. Increasing μ_2 , as previously mentioned, results in slower ECM degradation due to the increased renewal term and therefore the tumor cells

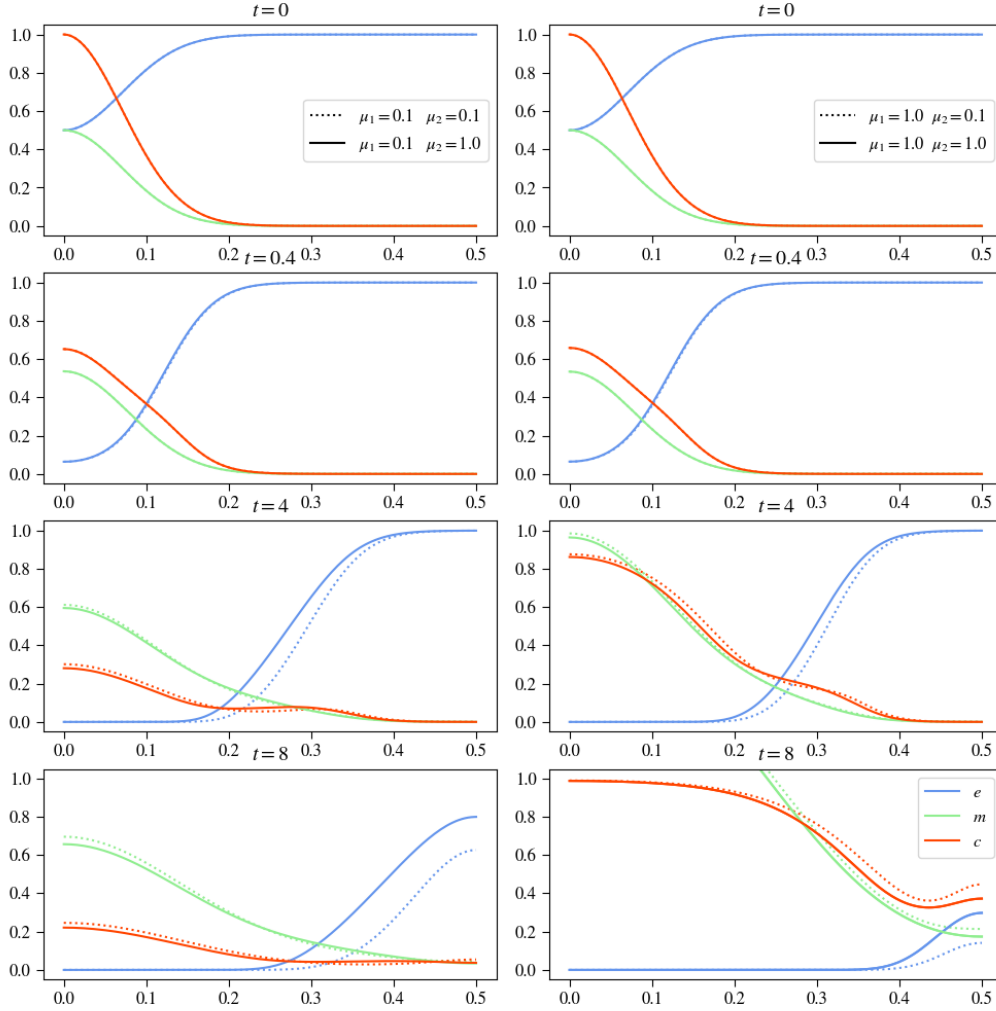


FIGURE 31. Plots show results for varying both μ_1 and μ_2 whilst keeping the other parameters constant.

are stretched out more evenly along the x-axis. Looking at the results when increasing μ_1 we also see the effects only after $t = 4$. For $\mu_2 = 0.1$ we see that the tumor cell density at $x = 0$ is slightly larger as well as at $x \approx 2.9$ the curve for $\mu_2 = 0.1$ is also slightly larger being a little below $\mu_2 = 1.0$ in between $x \approx 0.2$ and $x \approx 0.29$. The curve for the MDEs looks very similar in both cases for μ_2 due to the very similar tumor cell density curve, c , though the eECM has visibly faster degraded for $\mu_2 = 0.1$ due to the slower renewal.

$d_c - \gamma - \mu_1$ Variation

First we are going to take a look at how changing γ and μ_1 affects the system whilst having low diffusion values for the tumor cells with $d_c = 0.00005$, in figure 32. Inspecting the dotted curve on the left side column, shows the results for all parameters set to low, we see that diffusion is the main factor for the movement of the tumor cells, with only little influence of haptotaxis, the tumor cells staying with their maximum at the center. Because of this we also get a high MDE concentration there, but very little exceeding

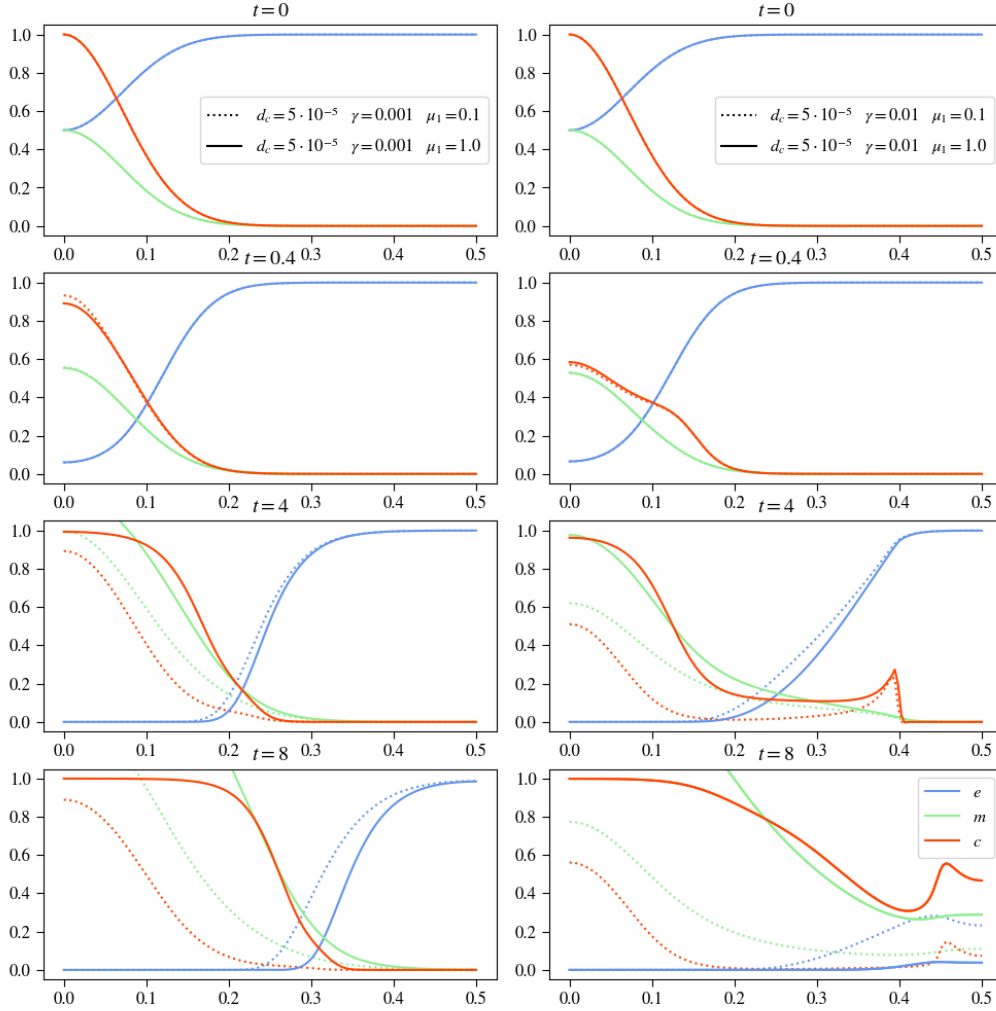


FIGURE 32. Plots show results for varying both d_c , γ and μ_1 whilst keeping the other parameters constant. This plot is the first of two, with the same d_c value for every plot in this figure.

the region past $x = 0.3$. Due to the MDE also staying centered around the origin the ECM there is completely degraded, though at $x = 0.4$ and further still completely there. Increasing the proliferation factor to $\mu_1 = 1.0$ shifts the tumor cell density rightwards, making proliferation also a factor for the cell density movement, though keeping the same shape as the low proliferation factor experiment. This right shift causes the MDE concentration to also shift to the right, leading to a faster ECM degradation. Comparing these two experiments already shows the influence of proliferation.

Taking now a look at the right column in figure 32 we see the effects of increased γ to $\gamma = 1.0$. Foremost we see for the tumor cell density a leading edge developing, separating it into two lumps, with one staying at the center the other invading the tissue and staying where $\nabla(c\nabla e)$ is highest. With increased μ_1 this secession moving into the tissue is getting more pointy, defying differentiability. After $t = 4$ we can observe clear differences regarding ECM and MDE concentration. We see that for higher μ_1 we also get a higher MDE concentration which degrades the ECM visibly faster at the end of the

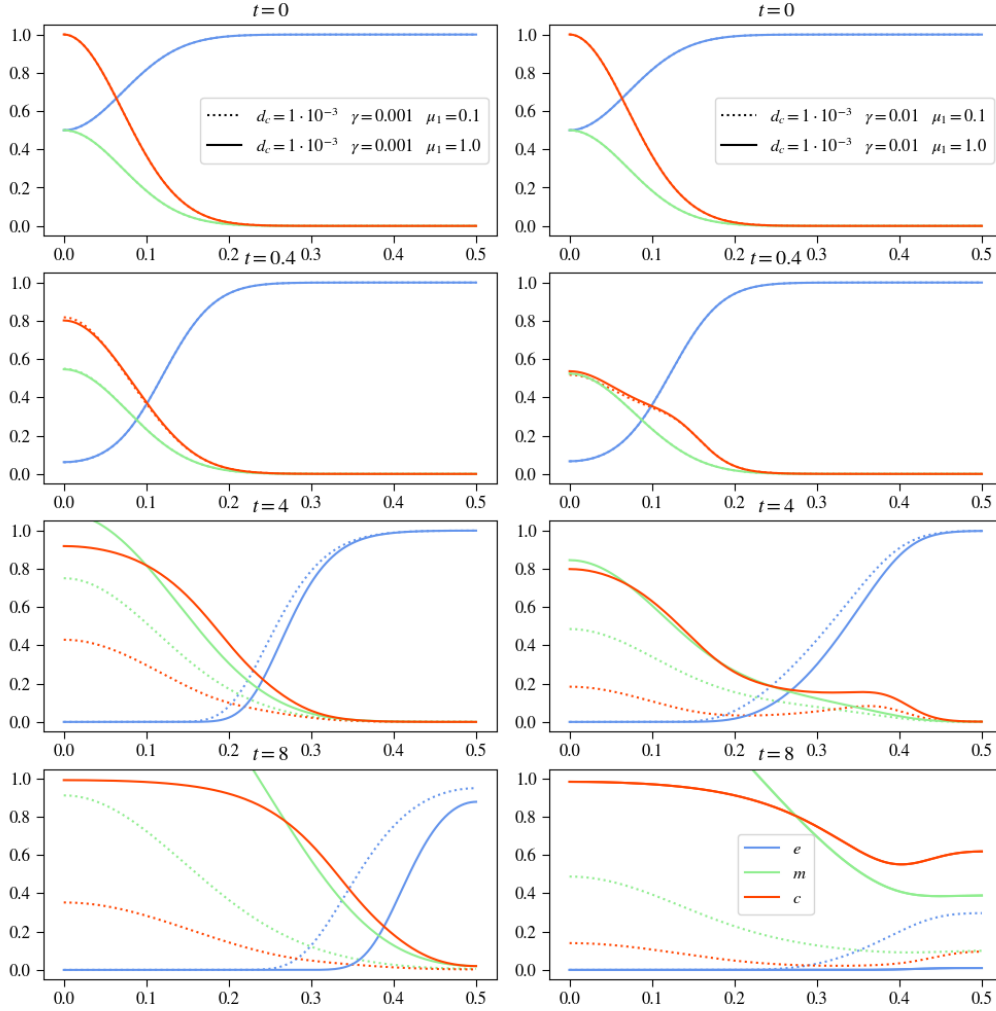


FIGURE 33. Plots show results for varying both d_c , γ and μ_1 whilst keeping the other parameters constant. This plot is the second of two, with the same d_c value for every plot in this figure.

experiments at $t = 8$. Though interestingly at $t = 4$ the ECM degradation difference is only minor, at the last point in time the accelerated tumor cell proliferation shows its effect with producing more MDEs and degrading the ECM considerably faster. What is also interesting to note is that increasing γ and keeping μ_1 low the total area of the MDE concentration is lowered also. Increasing now d_c to 0.1 we see for all experiments in figure 33 that the diffusion of the tumor cells was sufficiently high to evenly distribute the tumor cells constantly in the space. This constant distribution allows to get an even better look at how μ_1 affects the results, by seeing the lines, describing the tumor cells, rise through time. Looking at the tumor cells over time we can see no observable difference for varying γ . Haptotaxis effects are completely overlaid by diffusion. We see in the left column that if keeping d_c high and γ low, but increasing μ_1 leads to higher MDE production rates and also faster ECM degradation. The same behaviour is observable in the right column showing the results for high γ . That we see no difference is clear, since the tumor cell density development is identical over time as mentioned above.

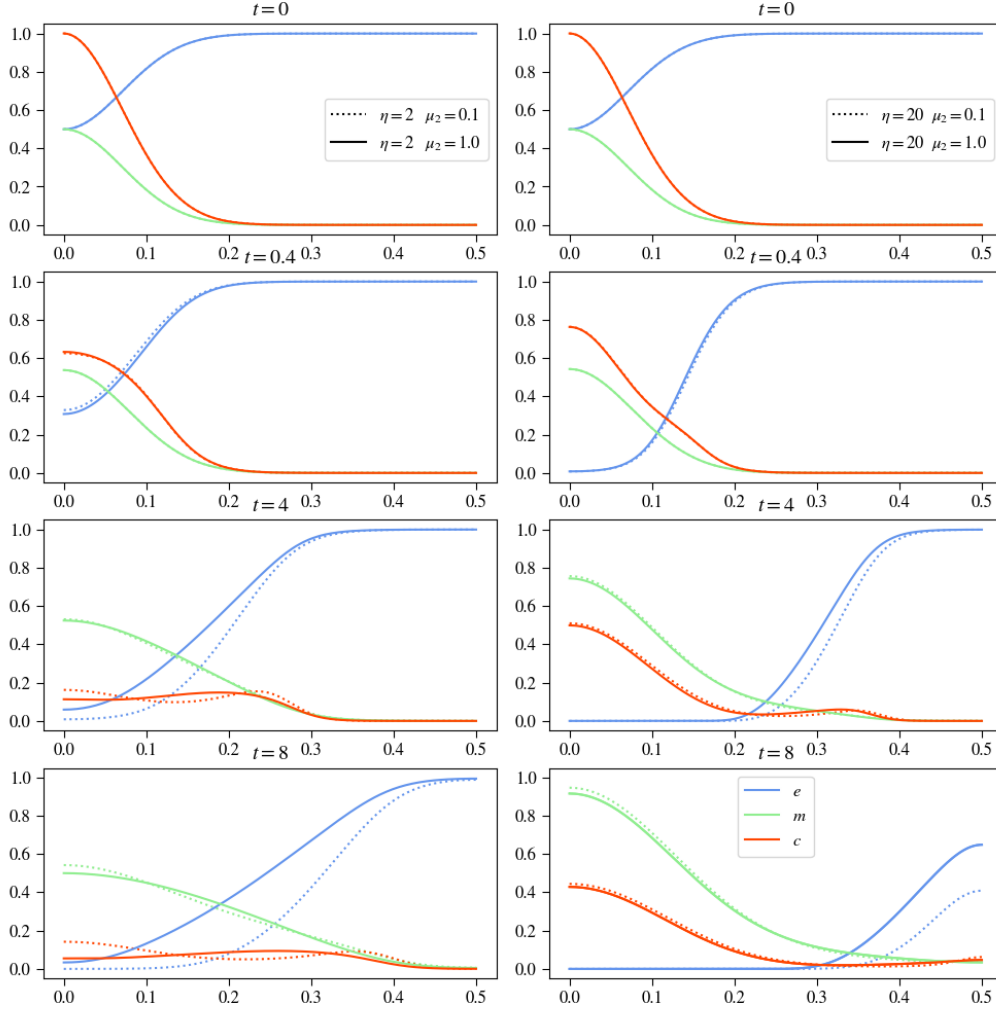
$\eta - \mu_2$ Variation

FIGURE 34. Plots show results for varying both η and μ_2 whilst keeping the other parameters constant.

Varying both η and μ_2 we can expect to see clear changes in the curve describing the ECM concentration. On the left side of figure 34 we can see the two experiments for low η values and see that increasing μ_1 has only a little effect. Where we could have expected to maybe even see an increase of the ECM we see that the ECM curves for both experiments verify that the renewal factor μ_2 was too low to counter the ECM degradation, even with a low degradation factor. Still between $\mu_2 = 0.1$ and $\mu_2 = 1.0$ there are visible differences in the degrading speed of the ECM. We can also observe that with the higher renewal term the tumor cell density curve receives more of an effect of haptotaxis resulting in a more stretched curve with only one long lump of tumor cells, where for the lower renewal factor we can still clearly see that there is a secession that invades the tissue and one that stays at the origin. Concerning the MDE curves we can see little difference, for higher μ_2 , which meant more stretched tumor cell density, we can also observe a more stretched MDE curve with a lower maximum at the origin.

Taking now a look at the experiments with raised η to accelerate the ECM degrading process, we can only see pregnant differences in the curve describing the ECM concentration, the other two look across the steps in time to be widely similar. For the ECM curve we see that the experiment with the lower μ_2 value results in a faster degradation process.

4.3 3D Results with Proliferation and Renewal - Homogenous ECM

4.3.1 Basecase Analysis

4.3.2 Parameter Analysis

Lorem ipsum dolor sit amet, consectetur adipiscing elit. Ut purus elit, vestibulum ut, placerat ac, adipiscing vitae, felis. Curabitur dictum gravida mauris. Nam arcu libero, nonummy eget, consectetur id, vulputate a, magna. Donec vehicula augue eu neque. Pellentesque habitant morbi tristique senectus et netus et malesuada fames ac turpis egestas. Mauris ut leo. Cras viverra metus rhoncus sem. Nulla et lectus vestibulum urna fringilla ultrices. Phasellus eu tellus sit amet tortor gravida placerat. Integer sapien est, iaculis in, pretium quis, viverra ac, nunc. Praesent eget sem vel leo ultrices bibendum. Aenean faucibus. Morbi dolor nulla, malesuada eu, pulvinar at, mollis ac, nulla. Curabitur auctor semper nulla. Donec varius orci eget risus. Duis nibh mi, congue eu, accumsan eleifend, sagittis quis, diam. Duis eget orci sit amet orci dignissim rutrum.

Nam dui ligula, fringilla a, euismod sodales, sollicitudin vel, wisi. Morbi auctor lorem non justo. Nam lacus libero, pretium at, lobortis vitae, ultricies et, tellus. Donec aliquet, tortor sed accumsan bibendum, erat ligula aliquet magna, vitae ornare odio metus a mi. Morbi ac orci et nisl hendrerit mollis. Suspendisse ut massa. Cras nec ante. Pellentesque a nulla. Cum sociis natoque penatibus et magnis dis parturient montes, nascetur ridiculus mus. Aliquam tincidunt urna. Nulla ullamcorper vestibulum turpis. Pellentesque cursus luctus mauris.

Nulla malesuada porttitor diam. Donec felis erat, congue non, volutpat at, tincidunt tristique, libero. Vivamus viverra fermentum felis. Donec nonummy pellentesque ante. Phasellus adipiscing semper elit. Proin fermentum massa ac quam. Sed diam turpis, molestie vitae, placerat a, molestie nec, leo. Maecenas lacinia. Nam ipsum ligula, eleifend at, accumsan nec, suscipit a, ipsum. Morbi blandit ligula feugiat magna. Nunc eleifend consequat lorem. Sed lacinia nulla vitae enim. Pellentesque tincidunt purus vel magna. Integer non enim. Praesent euismod nunc eu purus. Donec bibendum quam in tellus. Nullam cursus pulvinar lectus. Donec et mi. Nam vulputate metus eu enim. Vestibulum pellentesque felis eu massa.

4.4 2D Results with Proliferation and Renewal - Heterogenous ECM

In this section we are investigating how a more realistic structure of the ECM will affect the results of a simulation. We are still using the model with proliferation and renewal.

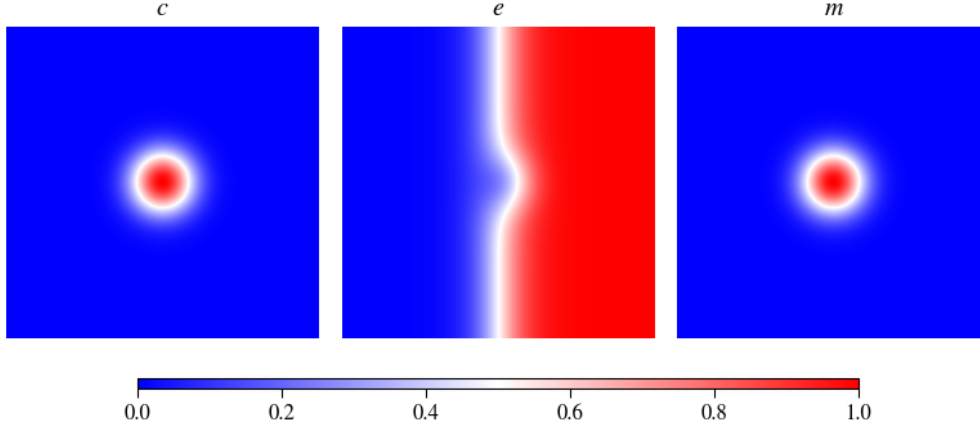


FIGURE 35. Visualization of the initial value distribution for an experiment in two space dimensions with a heterogeneous extracellular matrix

For this scenario we assume that there is a nodule of tumor cells already in the center of the simulation that has produced a concentration of matrix-degrading enzymes. Contrary to previous experiments we are assuming that the tumor cells are located at a basement membrane that they already have invaded and are now pushing into the extracellular matrix that lies behind it. These assumptions are described in figure ???. We model this in the following experiment with the initial conditions:

$$c(x, 0) = \exp\left(\frac{-(x - 0.5)^2}{0.01}\right)$$

$$m(x, 0) = 0.5c(x, 0) = 0.5 \exp\left(\frac{-(x - 0.5)^2}{0.01}\right)$$

$$e(x, 0) = 1 - 0.5c(x, 0)$$

insertcorrectecmdescription

Figure 36 you can see the effects using a heterogeneous extracellular matrix structure. The plots show in the left column the tumor cell density, the middle column the extracellular matrix concentration and on the right the matrix-degrading enzymes concentration. For the parameters we assumed the basecase studying the model with proliferation.

This experiment describes a more realistic biological scenario, like seen in figure ??, where the tumor cells are located at the basement membrane of neighboring tissue and have degraded this membrane to invade the surrounding tissue and degrade extracellular matrix there.

In the middle column's first image showing the initial distribution of the experiment you see that the extracellular matrix molecule concentration is only on the right side of the plot, this indicated the neighboring tissue to be invaded. In the center of the same image there is a hollow spot where the tumor cells of the initial distribution are located.

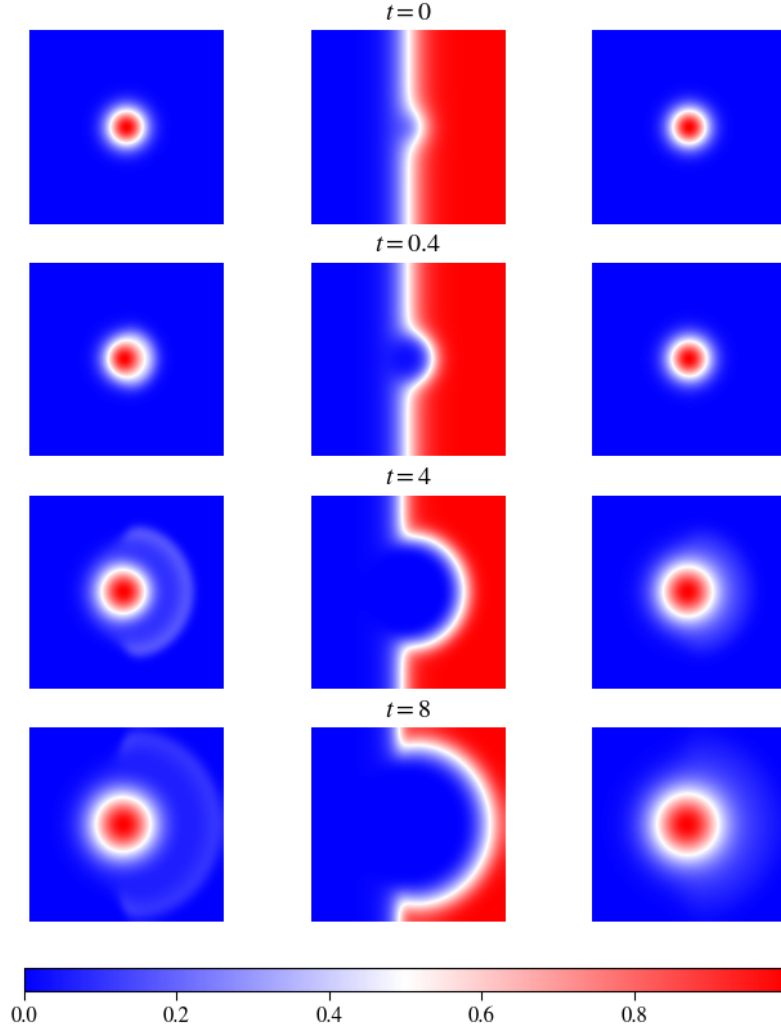


FIGURE 36. 2D Results using a heterogenous ECM with the parameter values: $d_c = 5 \cdot 10^{-4}$, $\gamma = 0.0055$, $\mu_1 = 0.1$, $\eta = 10$, $\mu_2 = 0.5$, $d_m = 1 \cdot 10^{-3}$, $\alpha = 0.3564$, $\beta = 0$; left: tumor cell density, middle: ECM concentration, right: MDE concentration.

After four timesteps you see that the ECM is slowly being degraded and the tumor cells are being pulled by the ECM concentration further into the neighboring tissue. The concentration of the matrix-degrading enzymes shows little differences comparing their behaviour to the experiments done with a homogenous ECM. They only depend indirectly on the ECM, by being produced where the tumor cells are being pulled by the extracellular matrix concentration.

The next point in time shows increased ECM degradation with also further invading tumor cells into the tissue. The tumor cells behave as a semicircular wave moving into the direction of the ECM, you can see the main lump remains at the center, with the edge of

having containinig a smaller amount of cells moving outwards. The image describing the matrix-degrading enzyme concentration shows still only minor effects, looking closely we can see that from the center moving to the right there is a slightly higher concentration of them than in the other direction.

The last row depicts the experiment after $t = 8$ timesteps and we see the aforementioned effects propagated. The ECM degradation has continued as well as the invasion of the tumor cells. The wave moving in direction of the remaining extracellular matrix molecules has spread through space and therefore decreased in its strength. The MDEs still show only little influence of the heterogenous ECM with the main lump staying centered and only difficult to recognize more concentration towards the movement of the tumor cells and concentration of the extracellular matrix.

Taking into account different extracellular matrix molecules and structure or physical influences as heat or radiation you can adjust the structure of the ECM and the behaviour of the system to better simulate reallife scenarios of cancer invading tissue.

4.5 3D Results with Proliferation and Renewal - Heterogenous ECM

5 Conclusion and Discussion

In this study, we conducted a parameter analysis for a numerical model in tumor development research. The aim was to investigate the impact of varying model parameters and dimensions on simulation outcomes and provide insights into the model's behavior under different conditions. This was done to facilitate implementing this model in a real-world scenario, facilitating an entry point for researchers to choose the parameters for their scenario.

The results of our analysis highlight the model's sensitivity to changes in key parameters, such as the diffusion coefficients on the tumor cells, the haptotactic coefficients, the proliferation rate of the tumor cells, the degradation rate of the extracellular matrix, and the production and decay rates for the matrix-degrading enzymes. We observed that small variations in these parameters can lead to significant differences in simulation outcomes, indicating the importance of carefully selecting and calibrating model parameters for accurate representation of biological phenomena.

Furthermore, our study revealed the complex interplay between different parameters during cross-varying them and their effects on tumor invasion and extracellular matrix degradation. For example, we found that increasing the haptotactic flux coefficient of the tumor cells is the critical component to controlling how many cells of a tumor invade the surrounding tissue and how many stay at the center of the simulation. Most of the parameters studied increased the invasion pace of the tumor cells and the degradation of the extracellular matrix.

Moreover, the influence of spatial dimensions on simulation outcomes was shown, with simulations in higher dimensions producing qualitatively different results compared to the initial one-dimensional model. This underscores the importance of considering the spatial complexity of biological systems when designing computational models for tumor development.

Additionally, our analysis sheds light on the limitations of the current model and areas for further improvement. The model could be extended in both discrete and continuous ways, for example, by implementing biochemical effects like chemotaxis, which is done in Kolev et al.'s work [12] or implement immune cell interactions or heterogeneity in tumor cell populations, to capture the complexity of the tumor microenvironment better.

In conclusion, our parameter analysis provides valuable insights into the behavior of the investigated numerical model in tumor development research and underscores the importance of parameter selection and model validation in mathematical oncology. By refining our understanding of the underlying mechanisms driving tumor progression, such models have the potential to inform therapeutic strategies and improve patient outcomes in the fight against cancer.

References

1. Anderson, A. Continuous and Discrete Mathematical Models of Tumor-induced Angiogenesis. en. *Bulletin of Mathematical Biology* **60**, 857–899. ISSN: 00928240. <http://link.springer.com/10.1006/bulm.1998.0042> (2023) (Sept. 1998).
2. Anderson, A. R. A., Chaplain, M. A. J., Newman, E. L., Steele, R. J. C. & Thompson, A. M. Mathematical Modelling of Tumour Invasion and Metastasis. en. *Journal of Theoretical Medicine* **2**, 129–154. ISSN: 1027-3662, 1607-8578. <http://www.hindawi.com/journals/cmmm/2000/490902/abs/> (2023) (2000).
3. Bekisz, S. & Geris, L. Cancer modeling: From mechanistic to data-driven approaches, and from fundamental insights to clinical applications. *Journal of Computational Science* **46**. 20 years of computational science, 101198. ISSN: 1877-7503. <https://www.sciencedirect.com/science/article/pii/S1877750320304993> (2020).
4. Hanahan, D. Hallmarks of Cancer: New Dimensions. *Cancer Discovery* **12**, 31–46. ISSN: 2159-8274. eprint: <https://aacrjournals.org/cancerdiscovery/article-pdf/12/1/31/3052722/31.pdf>. <https://doi.org/10.1158/2159-8290.CD-21-1059> (Jan. 2022).
5. Franssen, L. C., Lorenzi, T., Burgess, A. E. F. & Chaplain, M. A. J. A Mathematical Framework for Modelling the Metastatic Spread of Cancer. en. *Bulletin of Mathematical Biology* **81**, 1965–2010. ISSN: 0092-8240, 1522-9602. <http://link.springer.com/10.1007/s11538-019-00597-x> (2023) (June 2019).
6. Chaplain, M., Lolas, G. & ,The SIMBIOS Centre, Division of Mathematics, University of Dundee, Dundee DD1 4HN. Mathematical modelling of cancer invasion of tissue: dynamic heterogeneity. en. *Networks & Heterogeneous Media* **1**, 399–439. ISSN: 1556-181X. <http://aims sciences.org//article/doi/10.3934/nhm.2006.1.399> (2023) (2006).
7. Merino-Casallo, F., Gomez-Benito, M. J., Hervas-Raluy, S. & Garcia-Aznar, J. M. Unravelling cell migration: defining movement from the cell surface. en. *Cell Adh. Migr.* **16**, 25–64 (Dec. 2022).
8. Chaplain, M., McDougall, S. & Anderson, A. MATHEMATIC@ArticleKolev2010, author=Kolev, M. and Zubik-Kowal, B., title=Numerical Solutions for a Model of Tissue Invasion and Migration of Tumour Cells, journal=Computational and Mathematical Methods in Medicine, year=2010, month=Dec, day=30, publisher=Hindawi Publishing Corporation, volume=2011, pages=452320, abstract=The goal of this paper is to construct a new algorithm for the numerical simulations of the evolution of tumour invasion and metastasis. By means of mathematical model equations and their numerical solutions we investigate how cancer cells can produce and secrete matrixdegradative enzymes, degrade extracellular matrix, and invade due to diffusion and haptotactic migration. For the numerical simulationsof the interactions between the tumour cells and the surrounding tissue, we apply numerical approximations, which are spectrally accurateand based on small amounts of grid-points. Our numerical experiments illustrate the metastatic ability of tu-

- mour cells.,@article10.14492/hokmj/1520928060, author = Akio ITO, title = Large-time behavior of solutions to a tumor invasion model of Chaplain–Anderson type with quasi-variational structure, volume = 47, journal = Hokkaido Mathematical Journal, number = 1, publisher = Hokkaido University, Department of Mathematics, pages = 33 – 67, keywords = large-time behavior, quasi-variational structure, tumor invasion, year = 2018, doi = 10.14492/hokmj/1520928060, URL = <https://doi.org/10.14492/hokmj/1520928060> doi=10.1155/2011/452320, url=<https://doi.org/10.1155/2011/452320>
- AL MODELING OF TUMOR-INDUCED ANGIOGENESIS. en. *Annual Review of Biomedical Engineering* **8**, 233–257. ISSN: 1523-9829, 1545-4274. <https://www.annualreviews.org/doi/10.1146/annurev.bioeng.8.061505.095807> (2023) (Aug. 2006).
9. Klawonn, A., Köhler, M. & Rheinbach, O. HiFlow3 – A Hardware-Oriented Parallel Finite Element Package. *Innovative Parallel Computing, Proceedings of the 5th International Conference ParCo2001* **13**, 213–220 (2002).
 10. Kitware, Inc. *ParaView* <https://www.paraview.org/>. Zuletzt abgerufen am [Datum]. 2022.
 11. Stéphanou, A., McDougall, S., Anderson, A. & Chaplain, M. Mathematical modelling of the influence of blood rheological properties upon adaptative tumour-induced angiogenesis. *Mathematical and Computer Modelling* **44**. Advances in Business Modeling and Decision Technologies [pp. 1-95], 96–123. ISSN: 0895-7177. <https://www.sciencedirect.com/science/article/pii/S0895717705004565> (2006).
 12. Kolev, M. & Zubik-Kowal, B. Numerical Solutions for a Model of Tissue Invasion and Migration of Tumour Cells. *Computational and Mathematical Methods in Medicine* **2011**, 452320. ISSN: 1748-670X. <https://doi.org/10.1155/2011/452320> (Dec. 2010).
 13. Aznavoorian, S., Stracke, M., Krutzsch, H., Schiffmann, E. & Liotta, L. Signal transduction for chemotaxis and haptotaxis by matrix molecules in tumor cells. *The Journal of cell biology* **110**, 1427–38 (May 1990).
 14. Lu, P., Takai, K., Weaver, V. M. & Werb, Z. Extracellular matrix degradation and remodeling in development and disease. en. *Cold Spring Harb. Perspect. Biol.* **3**, a005058–a005058 (Dec. 2011).